Unraveling the Influence of Lipid Coating and Pluronic F68 on Monodisperse Microbubble Production at room temperature: Implications for Microbubble Coalescence, Stability and Acoustic Behavior

Ana Luísa Monteiro Walgode

Masters Dissertation

Master in Bioengineering - Biological Engineering

Supervisors

Prof. Dr. Klazina Kooiman and Prof. Dr. Maria do Carmo Pereira

Porto/Rotterdam, June 2023

Financial Support

Financial support from the Applied and Engineering Sciences (TTW) (Vidi-project 17543), part of NWO, and European Research Council under the European Union's Horizon 2020 research and innovation programme (Grant Agreement No 805308) is gratefully acknowledged.

Declaration

I hereby declare that this work is original and that all non-original contributions have been properly referenced with the identification of the source. I also declare that the Grammarly software provided by the University of Porto was used to revise the text for spelling, grammar, punctuation, and clarity.

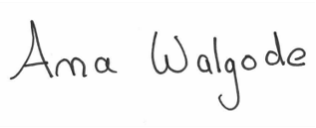

Ana Walgode, 16th June 2023

“I decided to see every problem as the opportunity to find a solution”

Walt Disney

Acknowledgments

These past years have been challenging, but at the same time, I am so grateful for everything that contributed to my growth. Whenever I take on a new challenge, I always give it my all, but this is not something that can be done alone.

In life, family comes first. To my dear dad, who is no longer with us, I know you' would be proud of your little engineer. To my amazing mom, who taught me to be the person I am today and has always been my side with so much love and understanding, thank you from the bottom of my heart. To one of my favorite persons, my dear and superhero brother, you are my true inspiration. You have always been there to support me and to make me so happy. To my uncle, who always loved me and stayed my side, thank you. I am proud to be the fourth one of the family to graduate in a university that means a lot to me.

Now, I would like to express my gratitude to Prof. Dr. Klazina Kooiman for accepting me for this project and for the warm welcome into your "bubble group". This experience was important for my professional and personal growth. Thank you for sharing your knowledge with me. A special mention goes to Prof. Dr. Maria do Carmo, an amazing teacher that shared so much knowledge during the past years and was always so understanding and helpful. To the PhD student Yuchen Wang, the one who was by my side each day, sharing knowledge and teaching me so many new laboratory protocols, I am grateful for the opportunity of working with you. To Hongchen, Sander, Gonzalo, Kirby, and Bram, a big thank you for your words and advice.

These acknowledgments wouldn't be complete without a word of appreciation to all my friends and colleagues who shared these years with me, whether it was studying together, stressing together, or laughing together.

Resumo

Ultrassom na área médica é amplamente utilizado para diagnóstico de imagem, no qual, os agentes de contraste de ultrassom emergiram para melhorar o contraste do sangue. As microbolhas (MBs), com um núcleo gasoso e um revestimento biocompatível, oferecem melhorias na ecogenicidade. No entanto, estas são comercializadas como suspensões polidispersas. Os dispositivos microfluídicos de fluxo focalizado permitem um maior controlo na produção de MBs monodispersas (monoMBs). No entanto, a ocorrência coalescência no chip, particularmente a elevadas taxas de produção, baixa concentração de lipídios, e a temperatura ambiente, limita a sua futura aplicação. Em trabalhos anteriores, a coalescência foi reduzida através da adição do copolímero Pluronic F68 (PF).

Este estudo teve como objetivo avaliar os efeitos do PF e de diferentes revestimentos lipídicos na produção de monoMBs livres de coalescência e na sua estabilidade ao longo de 7 dias. A capacidade de resposta acústica das monoMBs foi investigada. Além disso, a concentração de lipídios foi reduzida para 5 mg/mL, para explorar o potencial para futura implementação no mercado através de uma formulação mais económica. As MBs produzidas sem PF coalesceram no chip, resultando em suspensões polidispersas. Sem PF, a formulação DSPC: PEG40S: DPPE-PEG5000 mostrou melhoria na estabilidade em tamanho e concentração. A incorporação de 5, 7,2 e 10 mol% de PF resultou em monoMBs estáveis ao longo dos 7 dias e livres de coalescência, com raios variando de 2,04 a 2,52 µm. Uma maior mol% de PF resultou num incremento da taxa de redução de tamanho das monoMBs. No entanto, quando comparadas as monoMBs, o PF demonstrou não afetar a estabilidade de prateleira, exceto aquando da adição de 30 mol%, na qual, provavelmente, as monoMBs se dissolveram após 2 horas. Notavelmente, a redução na concentração de lipídios com a adição de 20 mol% de PF resultou em monoMBs estáveis ao longo dos 4 dias, com um raio de 1,10 µm. As monoMBs apresentaram capacidade de resposta acústica a 10 kPa, com frequências de ressonância à volta de 3 MHz e a rigidez média do revestimento variou entre 0,55 e 0,69 N/m.

Palavras-chave*:* Microbolhas monodispersas, Pluronic F68, Dispositivos microfluídicos de fluxo focalizado, Coalescência, Estabilidade de prateleira

Abstract

Medical ultrasound is widely used for diagnostic imaging, and ultrasound contrast agents have emerged to improve blood contrast. Microbubbles, with a gas core and a biocompatible shell, can offer enhanced echogenicity. However, commercially available microbubbles (MBs) are polydisperse suspensions. Flow-focusing microfluidic devices enable the precise control for monodisperse MB (monoMB) production, but on-chip coalescence, particularly at high production rates, lower lipid concentration, and room temperature, limiting further application. The addition of the copolymer Pluronic F68 (PF) had previously shown to decrease coalescence.

This study aimed to assess the effects of PF and different lipid coatings on coalescence-free production and shelf stability over 7 days. Acoustic responsiveness of monoMBs was investigated. Additionally, to explore the potential for future market implementation with a more cost-effective formulation, the lipid concentration was reduced to 5 mg/mL. MBs without PF coalesced in the outlet channel resulting in polydisperse suspensions. DSPC:PEG40S:DPPE-PEG5000 showed to improve shelf stability, in size and concentration. Incorporating 5, 7.2, and 10 mol% PF resulted in coalescence-free monoMBs with high shell stability over 7 days and radii ranging from 2.04 to 2.52 µm Higher mol% of PF caused higher shrinkage rates. However, comparing just the monoMBs, PF did not show to affect the shell stability, except at 30 mol% PF where it was assumed that the monoMBs completely dissolved after 2 h. Lower the lipid concentration with adding 20 mol% PF, result in stable monoMBs over 4 days with radius of 1.10 µm. The monoMBs had acoustic responsiveness at 10 kPa, with resonance frequencies around 3 MHz and a shell stiffness ranging from 0.55 to 0.69 N/m.

Key words: Monodisperse Microbubbles, Pluronic F68, Flow-focusing device, Coalescence, Shelf stability

Table of Contents

Abbreviations xiv

Symbols xv

1 Introduction 1

1.1 Current Challenges and Main Goals 2

1.2 Thesis output 3

2 Background 4

2.1 Microbubbles 4

2.1.1 Phospholipid-coated Microbubbles 5

2.1.2 Monodisperse vs Polydisperse Microbubbles 7

2.2 Monodisperse Microbubble Production 8

2.2.1 Flow-focusing Microfluidic Device 9

2.3 Microbubble Stability 10

2.3.1 Shrinkage Rate 11

2.3.2 Shelf Stability 12

2.4 Coalescence 12

2.4.1 Pluronic F68 14

2.5 Microbubble Acoustic Response 15

3 Materials & Methods 17

3.1 Production of Microfluidic Chips 17

3.2 Microbubble Formulations 18

3.3 Microbubble Production 20

3.3.1 Horizon Microbubble Maker 20

3.3.2 Imaging Setup 20

3.3.3 Chip geometry 21

3.3.4 Microbubble Production 21

3.4 Shelf Stability Measurement 22

3.5 Acoustical Characterization 23

3.6 Data Processing 24

4 Results 25

4.1 Microbubble Production 25

4.1.1 On-chip Size Distribution 26

4.2 Shelf Stability 27
4.2.1 Monodispersity Quantification 30
4.2.2 Size Stability Quantification 31
4.3 Shrinkage Rate 33
4.4 Attenuation Measurements 34
4.5 Lower the Lipid Concentration 36
5 Discussion 38
5.1 Coalescence 38
5.2 Shelf Stability 39
5.3 Shrinkage rate 41
5.4 Shell Stiffness 43
5.5 Limitations of the Study 43
6 Conclusions and Future Prospects 45
7 References 47

Abbreviations

3D - 3-Dimensional

CMC - Critical micelle concentration

C_3F_8 - Perfluoropropane

C_4F_{10} - Perfluorobutane

DPPA - 1,2-dihexadecanoyl-sn-glycero-3-phosphate

DPPC - 1,2-dipalmitoyl-*sn*-glycero-3-phosphocholine

DPPE - 1,2-dipalmitoyl-sn-glycero-3-phosphoethanolamine

DPPG - 1,2-dipalmitoyl-*sn*-glycero-3-phospho-(1'-*rac*-glycerol)

DSPC - 1,2-distearoyl-*sn*-glycero-3-phosphocholine

DSPE - 1,2-distearoyl-sn-glycero-3-phosphoethanolamine

FFMD - Microfluidic flow-focusing device

MB - Microbubble

MonoMB - Monodisperse microbubble

N_2 - Nitrogen

PEG - Polyethylene glycol

PEG2000 - Polyethylene glycol with molecular weight of 2000

PEG5000 - Polyethylene glycol with molecular weight of 5000

PEG40S - Polyoxyethylene-40-stearate

PEO - Polyethylene oxide

PF - Pluronic F68

PLGA - Polylactic-co-glycolic acid

PLA - Polylactic acid

PPO - Polypropylene oxide

PVA - Polyvinyl alcohol

SF_6 - Sulfur hexafluoride

UCA - Ultrasound contrast agent

US - Ultrasound

Symbols

χ – Shell stiffness

f_0 - Eigenfrequency

ω_0 - Angular eigenfrequency

$\sigma(R_0)$ - Surface tension at rest

P_0 - Ambient pressure

τ - Residence time

R_0 - Radius at resting size

κ - Polytropic gas exponent

ρ_L - Liquid density

1 Introduction

Medical ultrasound (US) is a prevalent diagnostic imaging method that can offer both anatomic and functional data in real-time [1]. It is used in clinical practice due to its safety, portability, and cost-effectiveness; in contrast to computed tomography and magnetic resonance imaging [1, 2]. However, it is difficult to visualize the blood due to its poor scattering properties. [3]. US contrast agents (UCAs) can improve blood contrast and contribute to applications in cancer diagnosis and cardiovascular disease [4]. The majority of UCAs are comprised of microbubbles (MBs), that in response to US, can produce a powerful echo that is several orders of magnitude higher than the solid particle of equivalent size, because of the high compressibility of the gas core [5].

MBs have a biocompatible shell that stabilizes a gas core with low solubility. The commercially available MBs are typically produced using traditional methods that results in polydisperse suspensions ranging from 1 to 10 μm in diameter [6]. These methods are simple and cost-effective and result in stable MBs with high efficiency, however, they lack the precision to control MB size and uniformity [7]. The US transducers are tailored to work in a limited frequency range that corresponds to the imaging application [1]. This results in only a small portion of MBs oscillating at their resonance frequency and, consequently, the generation of suboptimal echoes [8]. Therefore, is normally necessary to size sorting the polydisperse suspension of MBs before *in vivo* intravenous administration [9-11].

Flow-focusing microfluidic devices (FFMDs) permit high size control by adjusting the liquid and gas flow rates [41]. This thesis focuses on the production of phospholipid-coated monodisperse MBs (monoMBs), in a FFMD, as they are the most used for imaging and also a clinically approved for US contrast imaging and MB-mediated drug delivery, since they offer a good balance between MB stability and echogenicity [10].

1.1 Current Challenges and Main Goals

MonoMBs can be produced by FFMDs, however, at room temperature and high production rates, the coalescence probability in the outlet channel is high. [12]. Additionally, the freshly produced monoMBs are unstable and decrease in size [13]. One of the main challenges is to formulate a lipid: emulsifier coating with optimal ratios that can stabilize the MB shell and prevent coalescence [10]. Coalescence of MBs leads to wider size distributions and reduced the number of MBs that resonate at the driving US frequency [12]. Several strategies were identified to prevent coalescence during production in a FFMD, including increasing temperature [12], decreasing the production rate [13], increasing lipid concentration [14], and lastly, adding surfactant Pluronic F68 (PF) [15]. A previous study showed that the incorporation of PF can suppress MB coalescence however, the shelf stability was evaluated just over 10 min and there was a lack of acoustic characterizations [15].

Hence, the primary aim of this study was to assess the effects of PF and different lipid coatings on coalescence and shelf stability. Then, we investigated the acoustic responsiveness of the produced monoMBs to determine the influence of the studied coatings on the shell stiffness.

1.2 Thesis output

The research work for this thesis was performed at the department of Biomedical Engineering, Thoraxcenter, Erasmus MC University Medical Center Rotterdam, Rotterdam, the Netherlands.

This work resulted in the following output:

1. Accepted abstract for a poster presentation at the 2023 IEEE International Ultrasonics Symposium, to be held in Montreal, Canada from September 3-8 entitled *"Producing Coalescence-Free and Stable Monodisperse MBs at Room Temperature with Pluronic F68 Addition",* with Yuchen Wang[1], Sander Spiekhout[1], **Ana Walgode**[1], Benjamin R. G. Johnson[3], Antonius F. W. van der Steen[1,2], Klazina Kooiman[1]
2. Abstract submitted to the 9th Leeds Microbubble and Nanobubbles Symposium, to be held in Leed, UK, from July 17-19 entitled *"Producing Stable Monodisperse Microbubbles at Room Temperature with Pluronic F68",* with Yuchen Wang[1], Sander Spiekhout[1], **Ana Walgode**[1], Benjamin R. G. Johnson[3], Antonius F. W. van der Steen[1,2], Klazina Kooiman[1]
3. Will also result in a scientific paper that will be submitted in the present year, with Yuchen Wang[1], Sander Spiekhout[1], **Ana Walgode**[1], Benjamin R. G. Johnson[3], Antonius F. W. van der Steen[1,2], Klazina Kooiman[1]

[1]Department of Biomedical Engineering, Thoraxcenter, Erasmus MC, Rotterdam, NL

[2]Section of Medical Imaging, Department of Imaging Physics, Delft University of Technology, Delft, NL

[3]Molecular and Nanoscale Physics Group, School of Physics and Astronomy, University of Leeds, Leeds, UK

2 Background

2.1 Microbubbles

MBs, as UCA, can oscillate nonlinearly in response to US, therefore generating a harmonic signal that can be used for contrast enhanced US (CEUS) imaging (Figure 1). MB dynamics have intrigued scientists for more than a century. The first commercial UCA was the Albunex, which started being used in medical practice in 1993 [16, 17]. In the following decades, numerous alternative agents were developed with promising clinical applications [17]. MBs have a low solubility gas core stabilized by biocompatible shell, typically ranging from 1 to 10 µm in diameter, when produced by traditional methods [6]. They are the most commonly used UCA for diagnostic ultrasound imaging in clinical practice [8] and they can be injected intravenously at concentrations of 10^5 to 10^6 MBs/mL [10]. Due to their size, which is too large for extravasation but small enough to travel through the vasculature, MBs are a better option as a marker for blood flow [6, 18].

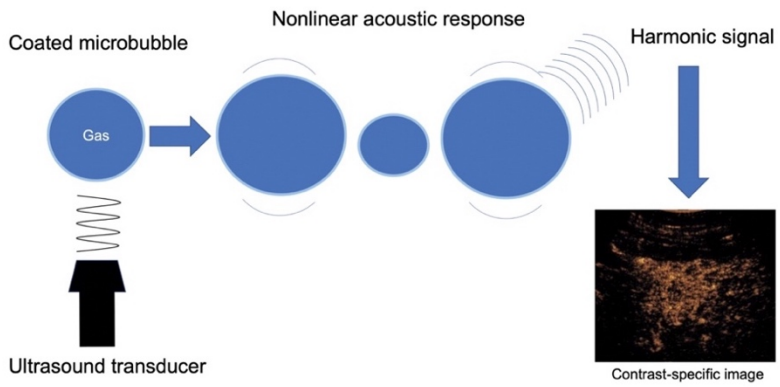

Figure 1 – An illustration of how MBs are used for CEUS. Adapted from [19].

To design a UCA is necessary to consider the imaging and therapeutic/theranostic properties of the agent, as well its pharmacokinetic characteristics to guarantee it can be used safely in medical applications. The gas core and coating shell is essential for MBs preserve their structural integrity and persistence in the bloodstream, meaning that the dissolution of the MB should be minimized. Originally, Albunex was filled with air [17], but by replacing the gas core with an inert gas that has low solubility in the liquid and

high molecular weight, the dissolution rate can also be reduced, and the MB's stability extended [20]. Low molecular weight gases more easily permeate into the fluid outside the shell [21]. The “second generation” of contrast agents commonly use nitrogen (N_2), and fluorinated gases such as sulfur hexafluoride (SF_6) and perfluorocarbons such as octafluoropropane (C_3F_8) and perfluorobutane (C_4F_{10}) [9].

The function of the shell coating is to prevent the dissolution of the gas, confer resistance properties, and decrease the interfacial surface tension [22]. MBs can be coated with proteins, phospholipids, or polymers [23]. The selection of the coating material is important and should be chosen for the specific application and desired characteristics, like stability, circulation time, imaging efficiency, and targeting ability [17]. Currently, the UCAs approved for clinical application are Definity (in Europe, Luminity), Sonazoid, Lumason (in Europe, SonoVue) and Optison [4]. Hard-shelled MBs are coated with cross-linked polymers, and have a robust and rigid coating that increase the MB stability and allow higher drug payload [24], although their voluminous structure can result in decreased drug delivery efficiency and lower ultrasound responsiveness [25]. There are some biocompatible polymers being tested, including polylactic acid (PLA) [26], polyvinyl alcohol (PVA) [27], and polylactic-co-glycolic acid (PLGA) [9]. However, these MBs are not commercially available [21]. Soft-shelled MBs are coated with phospholipids or proteins, and they exhibit a strong acoustic response due to their thin and flexible shell. Additionally, they display stable cavitation at low US amplitudes and disintegration or inertial cavitation at high amplitudes, which can lead to tissue permeabilization [24]. MBs can be stabilized using some proteins, including human serum albumin in the case of Optison, as well as oleosin and lysozyme, and these protein-stabilized MBs find applications in drug delivery, anticancer therapy, antibacterial activity, and biosensing [17].

2.1.1 Phospholipid-coated Microbubbles

Phospholipids, due to their amphiphilic properties and high biocompatibility as key components of cellular membranes, can form various types of particles, such as micelles and liposomes, by dispersing in water through the presence of two hydrophobic tails and a hydrophilic head [28]. The hydrophilic head is oriented to the exterior and interior of aqueous environments, while the hydrophobic tails are directed to the interior of the

bilayer [29]. A MB has the same liposome shell structure, but contains a gaseous core instead of an aqueous one and just one phospholipid layer (Figure 2) [30].

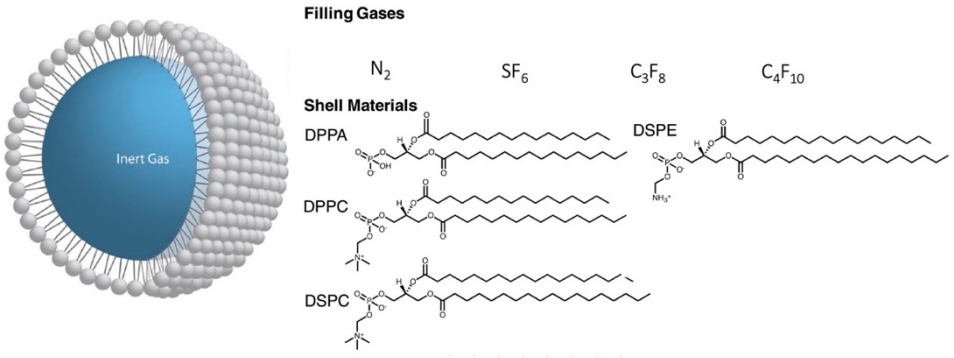

Figure 2 – Illustration of a MB with an inert gas core and phospholipid shell. The typically used filling gas and phospholipid. Adapted from [31].

A phospholipid-coated MB commonly have a monolayer of phospholipids (diacyl phospholipid with long and saturated acyl chains) as the main component such as 1,2-dipalmitoyl-sn-glycero-3-phosphocholine (DPPC), 1,2-dihexadecanoyl-sn-glycero-3-phosphate (DPPA), 1,2-distearoyl-sn-glycero-3-phosphocholine (DSPC), 1,2-dihexadecanoyl- sn-glycero-3-phospho-(1'-rac-glycerol) (DPPG) [30].

At a lower molar ratio in the shell formulation, emulsifiers are used. They are generally a lipid attached to a hydrophilic polymer moiety, such as polyethylene glycol (PEG). Popular used emulsifiers are polyoxyethylene-40-stearate (PEG40S), 1,2-distearoyl-sn-glycero-3-phosphoethanolamine-N-carboxy(polyethylene glycol) (DSPE-PEG2000), and 1,2-dipalmitoyl-sn-glycero-3-phosphoethanolamine(polyethylene glycol) (DPPE-PEG5000) [12-14, 32-34]. The emulsifier helps in the formation of the shell and create a layer that prevents coalescence and helps limiting the unwanted interactions with immune cells [30, 33]. For the production of targeted MB, it is common to add a PEG spacer arm like DSPE-PEG2000-biotin [30, 35]. Similar formulations to the clinically approved MBs have been explored and typically, the mixture is made of a 9:1 mole ratio of lipid to emulsifier [36-39], since it was found that a emulsifier content lower than 10% can be not enough to form a cohesive monolayer around the gas bubble [40].

The individual molecules within the shell can exist in either the liquid condensed (LC) or the liquid expanded (LE) phase. As the monolayer is compacted, resulting in a decrease in the area per molecule, some phospholipid molecules, such as DPPC (C16 tail) and DSPE-PEG2000, transitions from the LE to LC phase. However, DSPC (C18 tail) never changes

from LC, at room temperature, and PEG40-stearate is always in LE phase [40]. It is possible produce stable MBs with a cohesive coating if the condensed phase lipids are mixed with an appropriate quantity of emulsifier and form entangled microstructures [34].

2.1.2 Monodisperse vs Polydisperse Microbubbles

As above, standard MB production methods lead to polydisperse MB size distributions. In certain cases, the use of a polydispersity agent can be advantageous, such as when imaging multiple targets in the body simultaneously [10]. However, the transducers are work in just specific frequencies [1]. Thus, in a polydisperse suspension, only a fraction of the population is stimulated to the their resonance frequency [41]. Talu *et al.* [42] found that while only 49% of MBs in a polydisperse population had resonant frequencies in the transducer's bandwidth, a monodisperse population demonstrated 100% of efficiency. Additionally, it was shown that monoMBs had higher non-linear responses compared to the polydisperse MBs [43]. Therefore, monoMBs applied in ultrasound molecular imaging applications can improve the imaging sensitivity, by increasing it by a factor of two orders of magnitude [1]. Moreover, in imaging techniques like 3D super-resolution and plane wave imaging, where the concentration of MBs is limited, it becomes important to maximize the response of the MB population [10]. Furthermore, functionalized monoMBs that present a consistent and uniform acoustic response, can enhance the efficiency of drug delivery processes [10].

Researchers can benefit from the improved sensitivity and predictable behavior of monoMBs. This helps them better understand the physical properties and behavior of the monoMBs, which helps optimize medical treatments. In theragnostic applications is important to maximize the therapeutic effects, and at the same time, minimize the side effects, such as cell death or hemorrhage, allowing for local drug delivery either by opening the blood-brain barrier or by cell sonoporation [8]. The uniformity of monoMBs can be used to optimize the specific bonding with the ligand targets, making monoMBs promising for molecular imaging [46].

2.2 Monodisperse Microbubble Production

Figure 3 illustrates different methods to generate MBs with a uniform size distribution, using both indirect (a-d) and a direct approach (f).

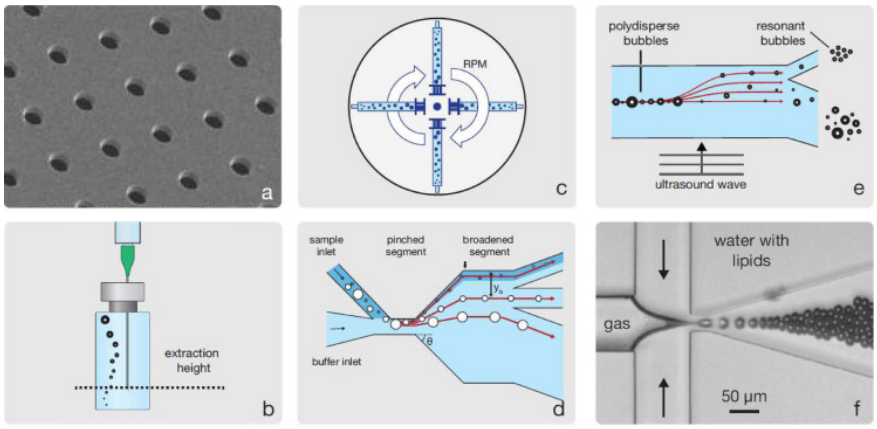

Figure 3 – Production methods for generating MBs with a uniform size distribution. Indirect methods: a) Pore filtration b) Decantation c) Centrifugation d) Pinched flow fractionation e) Acoustic MB sorting. Direct method: f) Flow-focusing device. Reprinted from [8].

In the indirect approach, a specific size range is isolated from the polydisperse MB suspension, which can be obtained via filtration (Figure 3 a) or size-sorting techniques, including decantation (Figure 3 b), centrifugation (Figure 3 c), and pinched flow fractionation (Figure 3 d) [8]. Mechanical filtration is a commonly used technique, where the polydisperse MB suspension is forced through a pore filter. However, the high pressures can damage the MBs, and the larger one possibly will deform and pass through the filter, reducing the homogeneity of the suspension [44, 45]. In size sorting techniques, different forces can be used to separate the MBs in terms of size [45]. The volume-dependent gravitational force is used to sort MBs either by decantation [46] or through few centrifugation steps [47]. However, the continuous MB sorting in microfluidic devices (MFDs), such as pinched flow fractionation, can give more control over the size distribution of MBs [10]. The method was developed by Yamada *et al.* [48] and involves the co-flow of MBs and a liquid, where the flow profile broadens at the boundary of the pinched segment and the particles are separated: the smaller particles are driven to the wall, while the larger particles flow to the center of the microchannel.

It is important to keep in mind that the achievement of uniformity does not always guarantee acoustic uniformity, because the resonance behavior of the MB is also affect by the coating [49]. MBs with identical sizes but different lipid packing densities can have

different non-linear viscoelastic shell behaviors, therefore, responding acoustically differently [50]. Segers *et al.* [44] introduced a microfluidic approach to sort MBs based on their acoustic resonance, rather than their size, where the resonant MBs to a traveling US wave were separated from the non-resonant MBs. Later, the same author confirmed the uniformity of the acoustically sorted MBs [50].

One advantage of sorting methods is the flexibility to choose the lipid composition for MB coating [10], which is important considering the limitations that exist for the formulations used in FFMDs to prevent on-chip coalescence.

2.2.1 Flow-focusing Microfluidic Device

MFD-based methods permit the direct production of monoMBs using minimal fluid volumes [51]. The MF channels facilitate the movement of the particles in a laminar flow [31]. T-junction (Figure 4 a) [52] and flow-focusing microfluidic devices (FFMDs) (Figure 4 b) are the most common used MFDs, with the main difference being the channels relative position [53]. Due to the T-junction perpendicular structure, it is difficulted to form MBs small enough for US applications, therefore, FFMDs are currently a more popular choice [31].

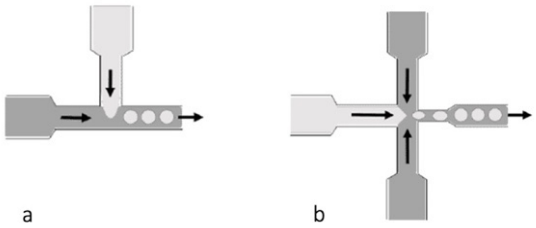

Figure 4 – MFDs for monoMB production. a) T-junction b) Flow-focusing. The light and dark grey represents the gas and the lipid solution, respectively.

The most common FFMD is designed with two continuous-phase channels positioned on either side of a gas-phase channel. The gas phase is focused in a narrow nozzle in the middle of the liquid two flow streams, which destabilizes and pinches off MBs [32]. Right after the nozzle, exist a V-shaped structure that allows fot the controlled production of individual MBs due to the flow gradient and the high shear forces [38]. The main way of tuning the on-chip size of MBs, involves the adjustment the liquid phase flow rates or/and the gas pressure [39]. Increasing gas pressure at a fixed liquid flow rate increases MB size and reducing liquid flow rate at constant pressure produces a similar effect [31]. In

addition, the width and height of the nozzle also impact MB size, i.e., by keeping a constant flow rate and pressure, widening the nozzle diameter results in larger MBs [38, 54].

2.3 Microbubble Stability

MBs can change their size over time through mechanisms such as coalescence, dissolution, growth, and Ostwald ripening [31]. The phenomenon of coalescence refers to the unification of two or more MBs into a larger MB. Dissolution occurs when the gas diffuses from the inside of the MB and dissolves to the surrounding solution. In contrast, growth involves the diffusion of gas to the inside of the MB from the solution. Finally, Ostwald ripening is a mechanism where the gas is transfered from smaller MBs to larger ones, due to differences in Laplace pressure [31]. To achieve the successful production of monoMBs, it is important to understand how MB stability can be improved. For monoMBs it can be both long-term stability, i.e, shelf stability, that focus on the stabilization process in a static environment, and short-term stability, i.e, coalescence during on-chip production. Moreover, depending on the application, investigating the acoustic and *in vivo* stability of the MBs is a further and important step to take in consideration[10].

In the FFMD, lipids in their expanded conformation adsorb to the gas thread (Figure 5, a), and the adsorption process reaches equilibrium before the nozzle because of the shear elongational flow along the interface [55]. Once the MB is formed, the total of lipids in the shell does not change during its stabilization [13, 14].

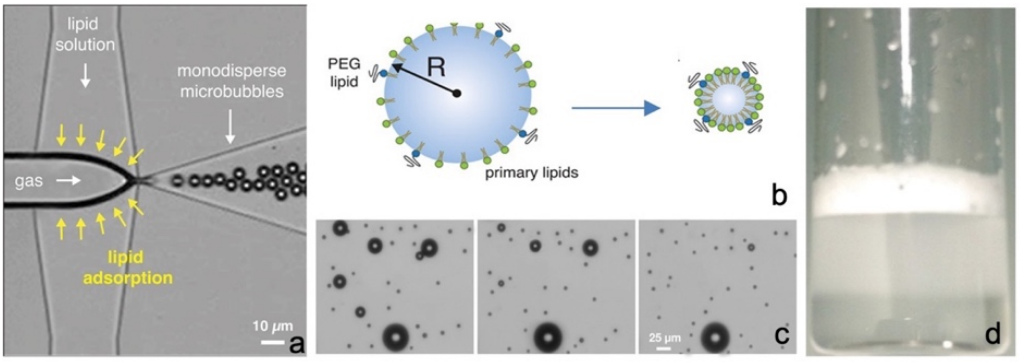

Figure 5 – Sequence of events during MB production and stabilization. a) Lipid adsorption b) MB dissolution c) MonoMB stabilization process d) MBs in a sealed vial stored after production. Adapted from [14].

The final size of a stable lipid-coated MB is always smaller than the size of the newly-formed unstable MB [12]. The curved interface in a spherical MB is defined by an energy per unit area called surface tension that leads to a pressure difference between the exterior and interior of the MB, known as Laplace pressure shown in Eq 1 [56, 57]. R is the MB radius and σ the MB surface tension.

$$\Delta P = \frac{2\sigma}{R} \quad \text{Eq 1}$$

MBs with small radii have a higher Laplace pressure, therefore is more probable that the gas is loosed to the surroundings, and subsequent diffusion of gas to larger MBs. This mass transfer mechanism, helps to minimize the global system surface energy, process named as Ostwald Ripening [56]. The shrinkage of the MB without any loss of lipids results in a more compactness monolayer (Figure 5, b). When the surface tension approaches zero, the dissolution process stops [40]. There are three primary factors contributing to the stabilization of MBs through adsorbed molecules. Firstly, the reduction in effective surface tension (σ) helps in MB stabilization by decreasing the pressure difference (ΔP) [58]. The Ostwald ripening process (Figure 5, c) makes the suspension polydisperse in the first 2 h [14, 39]. Due to the lower Laplace pressure, the bigger MBs acts as the sink for smaller MBs to release the extra gas before reach their final stable size, which in the end lead to big bubbles with size reach several hundred micrometers. When MBs reach their stable size, they can remain stable for days to months when stored in gas tight vial with the headspace filled with the same gas that is inside the MB [59, 60]. Figure 5-d shows the initial growth of foam at the top layer of the collected MBs, indicating the formation of larger MBs through Ostwald ripening. However, the foam decreases over time as most of the suspension becomes monodisperse.

2.3.1 Shrinkage Rate

The shrinkage rate of one MB is given by the ratio between the initial radius size R_i and the stable final radius size R_f, with stable MBs usually having a stable size small in 2-3 times [10]. Segers *et al.* [13] found that the shrinkage rate increases with the molar fraction and molecular weight of PEGylated lipids. The PEG chain expands in contact with a good cosolvent [61], therefore occupying a big area in the shell. For the MB to achieve the same final compressed monolayer, the area per molecule needs to decrease more,

resulting in a higher shrinkage rate [13]. The authors also observed that the ratio R_i/R_f is influenced by the concentration of ions in the solution and that the addition of TRIS buffer resulted in a lower shrinkage rate compared to pure water. On the other hand, the shrinkage rate is independent of the lipid concentration and production shear rate [14], temperature [12], and filling MB gas [13].

2.3.2 Shelf Stability

In terms of shelf stability, it was found that DPPC decrease the stability of the MBs when compared to DSPC [12]. This is due to the longer acyl chain of DSPC (18C) over DPPC (16C) that plays helps creating a more robust shell against dissolution[12, 62]. Talu *et al.* [54] also found that PEG40S is crucial to enhance shelf stability and prevent coalescence, and a mixture of DSPC/PEG40S provides excellent long-term stability for MBs, while MBs coated solely with DSPC or PEG40S experience complete dissolution. When the expanded phase of PEG40S resides between the condensed-phase regions of DSPC, it can assist in reducing the surface tension, in contrast to the single-phase observed in MBs coated with a single component [54]. Segers *et al.* [13] also discovered that the higher PEG molecular weights increased shelf stability. Regarding the gas core, while heavy gases than common gases like nitrogen and air can improve the stability, the inner gas choice has less impact on stability than the composition of the stabilizing shell [63].

2.4 Coalescence

The main problem for the synthesis of phospholipid-coated monoMBs is the coalescence phenomenon immediately after the nozzle or/and at the outlet of the FFMD [13]. The film drainage model explains the mechanism of coalescence as an initial approximation of the MBs by an external force that causes the decrease in the thickness of the thin film (film drainage). When the critical thickness is reached, the film becomes hydrodynamically unstable, leading to film rupture and formation of a coalesced [64, 65].

Lower production rate can suppress MB coalescence [12, 13, 31, 66]. At higher production rates, the inter-MB distance decreases, leading to stronger attractive forces that increase MB coalescence probability (Figure 6) [65]. Additionally, exists a correlation

between MB size and the occurrence of coalescence [67]. Nevertheless, high production rates are necessary to generate MBs with clinically relevant MB concentrations[14].

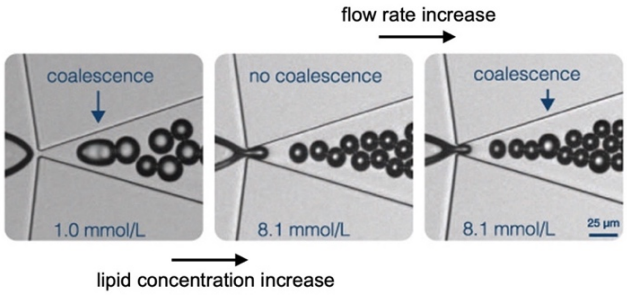

Figure 6 – Coalescence event. Increase of the flow rate result in the coalescence of MBs. Increasing the lipid concentration prevents coalescence. Adapted from [13].

High lipid concentrations are also necessary to mitigate on-chip MB coalescence at room temperature (Figure 6) [14]. These concentrations are normally increased by a factor of 10 compared to the traditional polydisperse MB production methods [10]. Interestingly, it was suggested that only a small fraction of the total lipids in the fluid (0.1 %) is responsible for forming the coating on the MBs [50]. The low efficiency of the phospholipid coating process, resulting in the loss of expensive materials, presents a disadvantage for implementation in the market. The efforts made by some authors [13, 53, 64] to decrease the lipid concentration have result in MB coalescence in the chip. The reason why is because the lipids that are not in the MB shell can form liposomes (diameters of 20-130 nm [12]) in the liquid film between newly formed MBs, therefore increasing the viscosity of the solution and creating additional forces with the MB shell making coalescence less probable to occur (Figure 7) [13]. Moreover, it was observed that the coalescence decreases with increasing PEG molecular weight and PEG molar fraction [13].

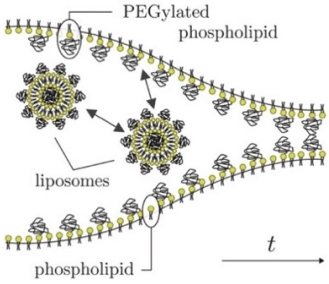

Figure 7- PEGylated liposomes are present in the film that forms between two MBs coated with PEGylated phospholipids. As time (t) progresses, the film gradually becomes thinner, thereby increasing the probability of coalescence. The arrow represents the intermolecular forces between the liposomes as well as between the liposomes and the surface of the MB. Adapted from [13].

2.4.1 Pluronic F68

PF, also known as polaxamer, is a nonionic copolymer consisting of a triblock structure of PEO-PPO-PEO (polyethylene oxide (PEO) and polypropylene oxide (PPO)). PF possesses amphiphilic properties due to the constituent blocks, PEO and PPO, which are hydrophilic and hydrophobic, respectively [68]. This copolymer is widely employed as a surfactant and when reaching or surpassing the critical micelle concentration (cmc), spontaneously assemble into micelles [69, 70]. These polymers have also gained attention over conventional copolymers because of some advantages properties, like the high surface activity, low toxicity, and good biocompatibility and biodegradability [70]. PF-68 and -127 are particularly relevant for therapeutic applications [70-77]. It has been observed that different PFs can intercalate with the lipid monolayers, leading to a V-shaped configuration (Figure 8). The central PPO chains of PF interact with the hydrophobic portion of lipids, while the outer PPO segments interact with the hydrophilic groups of lipids. This intercalation can improve MB stability by reducing surface tension [78, 79]. One study [78] also proposed that as the lipid molecules pack more tightly during shell stabilization, some components can be expelled at the same time, such as PF [78]. Additionally, it was observed that in different PFs, the polymer escaped from the monolayer at lower temperatures, indicating that the configuration of PF is a function of temperature [79].

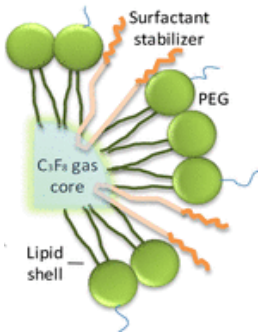

Figure 8 – Conformation of PF in a phospholipid MB shell. Reprinted from [78].

Studies were performed in FFMDs for MB production with the addition of PF. Shih *et al.* [15] showed that adding PF to a lipid solution helped suppressed MB coalescence (Figure 9). However, the stability was just measure over 10 min and lacked the acoustic characterization. Zhuo Chen *et al.* [80] did a study on the stability and acoustic characteristics of oleosin MBs, where with incorporation of PF in size-stable monoMBs

over 2-3 weeks, without significant dissolution or coalescence. The study also highlighted that the characteristics of the MB shell could be regulated by adjusting the PF structure in which a big amount of PF, led to more hydrophilic domains, and resulted in stiffer shell. Other study [81] using oleosin/PFs, showed that the PF better prevent coalescence over other species of PFs. The MBs were stable over 4 weeks, with no observable changes in size even after 5 days. One theory proposed by the authors is that the presence of PF in the solution helps to lower the surface tension and also to form the coating of the MBs upon their formation at the nozzle. Then, in the outlet channel, oleosin begin the adsorption process onto the MB surface, potentially displacing some of the PF.

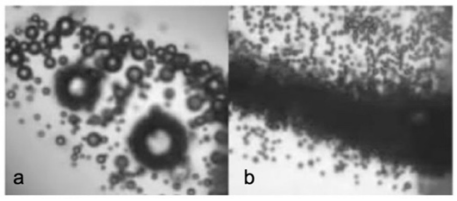

Figure 9 – Adding PF to the lipid solution reduce MB coalescence. a) no PF b) addition of PF. Reprinted from [15].

2.5 Microbubble Acoustic Response

US imaging operates by generating ultrasound waves and receiving their echoes through a transducer [82]. MBs can oscillate in a nonlinear way as the gas core expands and compresses [83]. Consequently, the acoustic response of MBs produces a a more powerful echo compared to a rigid particle of equal size [84]. The size of the MB appropriated for clinical applications match with resonance frequencies ranging from 1 to 10 MHz, which is inside common frequencies interval used in US imaging [3]. Enhanced resolution can be achieve with higher frequencies due to shorter wavelengths, while imaging depth decreases with higher frequencies due to the attenuation effect [9]. At low-pressure, MBs show a linear response where the amplitude of oscillation that is directly proportional to the applied acoustic pressure at the fundamental frequency [85]. Nevertheless, is the non-linear oscillation at harmonic and subharmonic frequencies that make MBs relevant as an UCA [86].

The presence of a coating influences the viscoelastic properties of the shell, such as its stiffness (shell elasticity). This elasticity will lead to an increase in the resonance frequency, when compared with an uncoated gas MB [8, 87]. The oscillation amplitude

of MBs is higher in response to a particular frequency, known as the resonance frequency or eigenfrequency. The eigenfrequency, f_0 , of a coated MB in the elastic mode can be determined for small amplitude oscillations using the angular eigenfrequency, ω_0, according to Eq 2 [3],

$$\omega_0 = 2\pi f_0 = \frac{1}{R_0}\sqrt{\frac{1}{\rho L}\left(3\kappa \mathrm{P}_0 + (3\kappa - 1)\frac{2\sigma(R_0)}{R_0} + \frac{4\chi}{R_0}\right)} \qquad \text{Eq 2}$$

where χ represents the shell stiffness, R_0 corresponds to the radius at resting size, and $\sigma(R_0) = 0.02$ N/m is the surface tension of the MB at rest. Follows the ambient pressure $\mathrm{P}_0 = 1 \times 10^5$ kPa; liquid density $\rho_L = 1000$ kg/m^3 for water; and C_4F_{10}. polytropic gas exponent $\kappa = 1.07$. The equation shows an inverse relationship between the size of the MB and its corresponding eigenfrequency, indicating that smaller MBs have higher eigenfrequencies.

3 Materials & Methods

3.1 Production of Microfluidic Chips

The master mold of the polydimethylsiloxane (PDMS) microfluidic devices (chips) was provided by the University of Leeds for this study. The microfluidic chips were casted as illustrated in Figure 10.

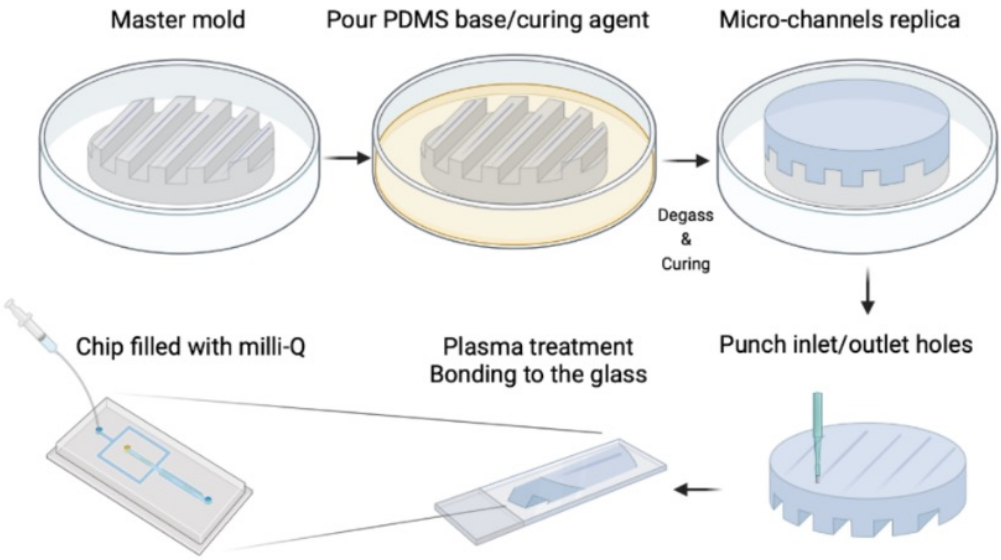

Figure 10 – Fabrication of PDMS flow-focusing microfluidic chip.

PDMS chips were fabricated by pouring a 10:1 mixture of Sylgard 184 (Dow Corning, the Netherlands) PDMS and curing agent onto the master mold. Subsequently, the PDMS was degassed in a vacuum chamber for 40 min and then cured on a heating pad at 75 °C for 1 h. The PDMS layer was then peeled off from the master, resulting in a replica of the channels on the solid gel block which were then cut to the size of the individual chips. To enable the injection of the liquid phase and gas phase to the channel afterwards, two inlet holes and one outlet hole were punched using a 1 mm diameter biopsy punch. Subsequently, the channel was bonded to a microscope slide through air plasma treatment (HPT, Runcorn, UK) for 1 min on 60% power. The chip was then baking at 95 °C for 3 min to accelerate the bondage process, followed by a 5 min plasma treatment at 80% power to restore hydrophilicity of the channel. Immediately after treatment, the channel was filled with water (milli-Q, Millipore) to preserve the hydrophilicity. The chip

was stored in milli-Q water to prevent evaporation of the water in the channel. Figure 11 shows two images of the microfluidic chips captured during and after the aforementioned process.

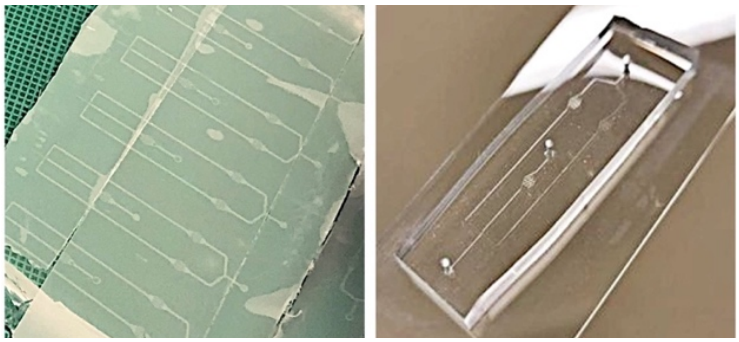

Figure 11 – Images of the in-house produced microfluidic chips. Multiple chips are shown on the left, replicated from the master mold. On the right, a chip after plasma treatment and bonding to the glass.

3.2 Microbubble Formulations

In this study, 12 variations of 3 lipid formulations were investigated. The first formulation, referred to as Formulation 1, consisted of a mixture of DSPC and DPPE-PEG5000 (DPPE-PEG5K), (Lipoid GmbH, Ludwigshafen, Germany), at 9 to 1 molar ratio. This formulation was previously utilized by Segers *et al.* [32], for the production of monodisperse microbubbles. Formulation 2 was built upon Formulation 1 (F1) with adding PEG40-stearate (PEG40S), (Sigma-Aldrich, Zwijndrecht, the Netherlands). The molar ratio of lipids in Formulation 2 (F2) was adjusted to DSPC:PEG40-stearate:DPPE-PEG5000 = 82.1:7.9:10. Formulation 3 (F3) was further modified on formulation 2 by substitute DPPE-PEG5000 with DSPE-PEG5000 (DSPE-PEG5k), (Bio-connect, Huissen, the Netherlands), while keeping the molar ratio between lipids unchanged.

For monoMB production, the lipids were prepared with indirect method as described before [49]. Briefly, lipids were combined as the molar ratio mentioned above, dissolved in chloroform/methanol at 9:1 vol/vol, and evaporated under argon gas (Linde Gas Benelux, Schiedam, the Netherlands). The resulting film was then dried under vacuum overnight and stored at -20 °C.

On the day of MB production, the lipid film was rehydrated in 55 °C PBS (Gicbo, USA) and incubated in a 55 °C water bath for 40 min, with vertexing every 10 min. Subsequently, Pluronic F68 (PF68™, Gicbo, USA) hereafter referred to as PF, was added

to the lipid solution to reach the final lipid concentration of 20 mg/mL. The amount of PF added varied based on the desired molar ratio (0%, 5%, 7.2%, 10%, and 30%) for each formulation. The solution was then subjected to sonication in a sonication bath at 55 °C for 20 min, followed by cooling to room temperature. Additionally, F2 with 20 mol% PF: DSPC:PEG40S:DPPE-PEG5K:20PF was studied to explore the possibility of producing monoMBS at a lower lipid concentration of 5 mg/mL. Table 1 provides a summary of the investigated formulations.

Table 1 – Lipid formulations with the mol% of each component and their corresponding simplified MB names were assigned based on specific criteria. F1, F2, and F3 represent the lipid formulation for each MB. The first digit in the name indicates the mol% of PF68, and PF68 is abbreviated as PF. "MB" is added to indicate MB. All MB have a lipid concentration of 20 mg/mL expect that last in the table with 5 mg/mL.

MB name	DSPC	PEG40S	DPPE-PEG5K	DSPE-PEG5K	PF
Formulation 1 : DSPC:DPPE-PEG5000 = 9:1					
F1:0PF-MB	90	-	10	-	0
F1:5-MB	85.5	-	9.5	-	5
F1:7.2-MB	83.5	-	9.3	-	7.2
F1:10-MB	81	-	9	-	10
F1:30-MB	63	-	7	-	30
Formulation 2 : DSPC:PEG40-S:DPPE-PEG5000 = 82.1:7.9:10					
F2:0PF-MB	82.1	7.9	10	-	0
F2:5PF-MB	78	7.5	9.5	-	5
F2:7.2PF-MB	76.2	7.3	9.3	-	7.2
F2:10PF-MB	73.9	7.1	9	-	10
F2:30PF-MB	57.5	5.5	7	-	30
Formulation 3 : DSPC:PEG40-stearate:DSPE-PEG5000 = 82.1:7.9:10					
F3:7.2PF-MB	76.2	7.3	-	9.73	7.2
Lower lipid concentration to 5 mg/ml					
F2:20PF-MB	65.7	6.3	8	-	20

3.3 Microbubble Production

3.3.1 Horizon Microbubble Maker

The Horizon instrument (Figure 12) is a microfluidic system that can be used for production of monoMBs. Briefly, the gas pressure regulator controls the C4F10 supply, and two P-pumps connected with thermal-flowmeters allowed for a controllable and non-pulsatile flow (± 0.1 µL/min) of the liquid solution. Additionally, a 0.5 µm in-line filter was integrate in the system to prevent blockage problem. Both gas and lipids were conducted through two inlet tubings and connected to the microfluidic chip, while one outlet tubing collected the MBs in an inverted vial. The chip was placed on a custom holder and securely fastened with a manifold on a platform that can be manually adjusted.

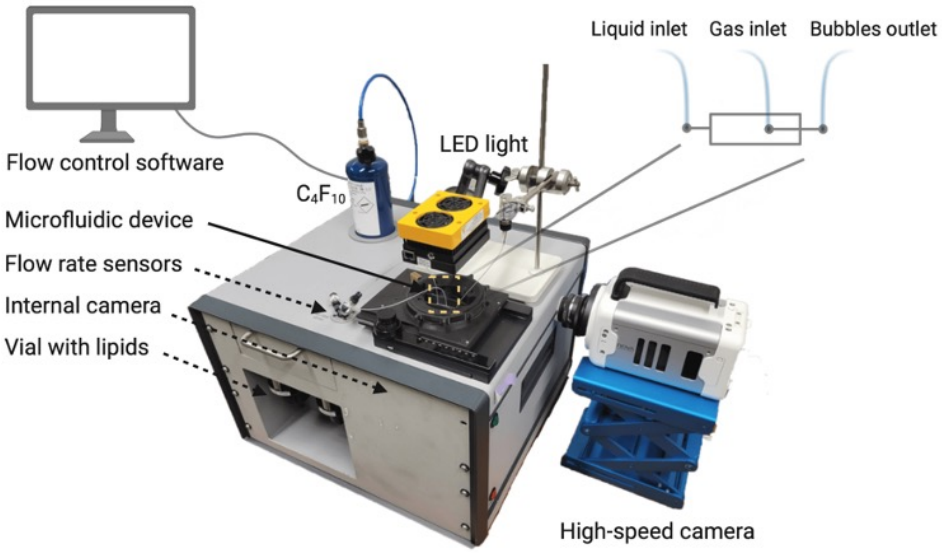

Figure 12 - Image of Horizon MB maker with labels highlighting its major components: gas supply, holders for the vial with the lipids and for the chip, and optical microscopy. The dashed arrows indicate internal elements within the system (flow rate sensors and an internal camera) as well as the insertion point for the vial containing the lipids. A schematic illustrating the tubing connection with the chip is provided. The system also integrates external components (high-speed camera, LED light, and computer).

3.3.2 Imaging Setup

The integrated optical system of the Horizon instrument consists of Kohler coaxial illumination system and a 20x objective arranged in an inverted configuration. To monitor the on-chip MB production, a high-speed camera (FASTCAM NOVA, Photron) with 20.0 µm pixel size was connected to the Horizon. The camera typically operated at frame rates

of 200 Kfps and 600 Kfps, with an external high-intensity LED light for illumination during high-speed imaging.

3.3.3 Chip geometry

MBs were generated in a flow-focusing chip with a channel depth of 25 µm and a 5 ± 0.5 µm wide nozzle, which enlarged to an outlet channel with a width of 60 µm length of 2000 µm as shown in Figure 13. The width of the nozzle was consistently measured before using a new chip to ensure the accuracy of the dimensions.

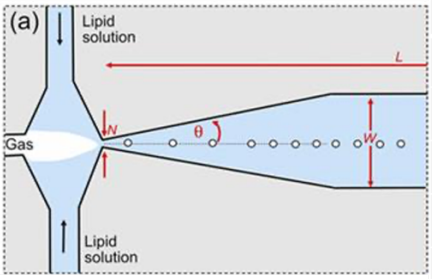

Microfluidic Chip Parameters	
Nozzle width, N	5 µm
Channel width, W	60 µm
Channel depth, D	25 µm
Length of outlet, L	2000 µm
Outlet angle, θ	15 °

Figure 13 – Schematic of the FFMD design made by the University of Leeds with dimensions in the accompanying table [88].

3.3.4 Microbubble Production

All MBs in this study were produced at room temperature with a C_4F_{10} gas (Perfluorobutane, F2 Chemicals Ltd, Preston, UK) pressure of 800 mbar. During production, high-speed imaging at 200–600 Kfps was recorded to monitor production over time at the nozzle. A custom-developed MATLAB (The MathWorks, Natick, MA, USA) script (Figure 14) was employed to measure the on-chip size distribution of the formed MBs on the rectangular section immediately after the nozzle.

To ensure comparability among MBs, preliminary experiments were conducted to determine the shrinkage rate of PF-containing MBs, enabling accurate prediction of their final stable sizes. It was established that the shrinkage rate is determined by the coating formulation and remains independent of the gas pressure and liquid flow rate applied during the process [13]. Considering the experimentally obtained shrinkage rate values of 2-3, and the frequency range supported by the in-house acoustic setup (1-5 MHz), the initial on-chip radius of the MBs was set at approximately 6 µm, which, with subsequent shrinkage of 2-3 times, resulted in a final radius of 2-3 µm (bigger MBs would resonate

below 1 MHz and smaller MBs tend to be less stable [9]. Therefore, the liquid flow rate was adjusted to produce MBs with an on-chip peak radius around 6 µm.

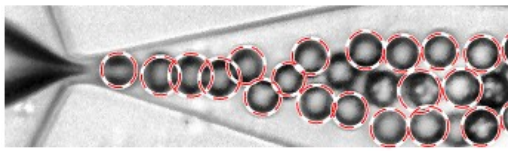

Figure 14 – On-chip size distribution measurements with a MATLAB script.

To collect the MBs, the outlet of the chip was connected to a 19G needle. A ventilation needle was inserted into the bottom of the medical vial, which was positioned upside-down (Figure 15, b). The MBs formed during the process were collected in a gas tight medical vial, which had previously been sealed with a rubber stopper and filled with C_4F_{10} gas in the headspace. After collecting 1 mL of MBs, the needles were disconnected, and the vial was placed upright at room temperature to allow the MBs to stabilize (Figure 15, c). An example of a high-speed imaging during MB production is shown Figure 15, d.

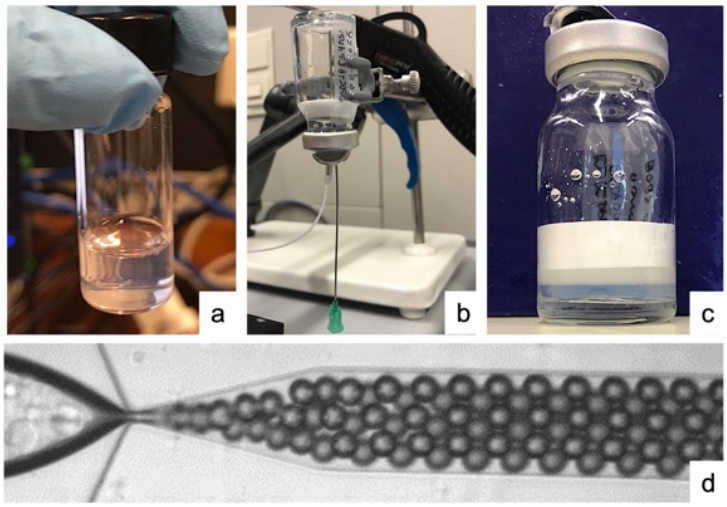

Figure 15 – Production of MD-MBs. Panels a), b), and c) depict photographs of the sequential process, including the prepared lipid solution, the setup for MB collection, and the MBs after production, respectively. Panel d) exhibits a bright-field image of a high-speed video captured at a frame rate of 200 kfps, during F1:7.2PF-MB formation.

3.4 Shelf Stability Measurement

The shelf stability was assessed using a Coulter Counter Multisizer 3 (Beckman Coulter, Mijdrecht, the Netherlands) to measure the size distribution measured 2 h, 1 d, 2 d, 4 d, and 7 d. The starting point, t=0, was defined as the moment when the collection of 1 mL of MBs in the sealed vial was concluded. For the quantification of particles ranging from

1 to 30 µm in diameter, 50 µm aperture tube was used. A waiting period of 3 min was implemented before the initial measurement to allow for MB stabilization in the filtered Isotone II diluent (Beckman Coulter, Mijdrecht, the Netherlands).

3.5 Acoustical Characterization

Figure 16 illustrates the schematic representation of the transmission setup employed. The attenuation curves were measured 2 d after MB production, and the attenuation values (Y-axis) were normalized to eliminate the influence of the number of MBs. The measurements were conducted at an acoustic pressure of 10 kPa, with the objective of determining the stiffness parameter. The stiffness of the shell is determined by the low-pressure response (10 kPa), and is responsible for establishing the eigenfrequency of the MB oscillations with elastic behavior [50]

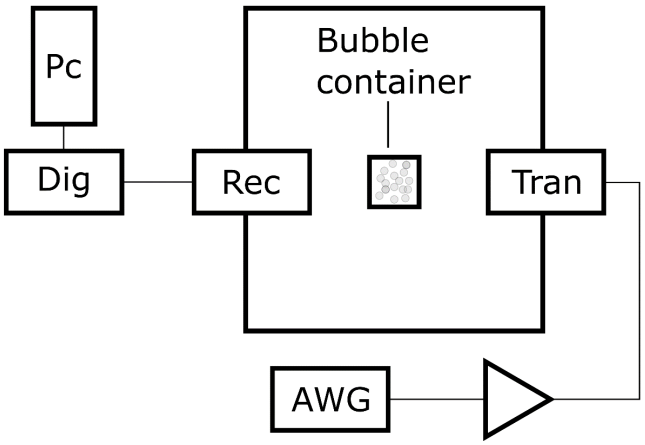

Figure 16 – Scheme of the setup used for attenuation measurements.

A volume of 0.2 µL of MB solution was mixed with 100 mL saline-buffered solution (Isotone-II, Beckman Coulter), and 30 mL was added to the MB container (2.4 x 2.4 cm) which contained a rotating magnetic stirrer.

After 3 minutes a sequence of acoustical pulses ranging in frequency from 1 to 5 MHz, in 100 kHz increments were transmitted at a pressure level of 10 kPa (41 pulses total). This was accomplished using a waveform generator in an arbitrary mode (AWG) (WW2572A, 250 MS/s, Tabor Electronics, Tel Hanan, Israel), amplifier (310L, ENI, Rochester, NY, USA) and transmitting transducer (Tran) (PA081, Precision Acoustics, Dorchester, UK). The pulses were 12 cycles, tapered with a Tukey window over the first

2 cycles and the last 2 cycles. Consecutive pulses were separated by a 300 µs rest period. The acoustical signal was received by a receiving transducer (Rec) (PA275, Precision Acoustics, Dorchester, UK) and digitized (Dig) (M4x.4420-x4, Spectrum Instrumentation, Limerick, Ireland) without amplification and stored on a computer (Pc).

The acoustical measurement was performed 10 times on the same MB sample at 5 s intervals to avoid repeated insonications. The entire measurement procedure was repeated 3 times on a fresh MB sample. To obtain the attenuation spectra, the magnitude of the individual pulses was dived by those measured from a sample without MBs in the frequency domain and averaged over the 10 measurements.

3.6 Data Processing

The shrinkage rate of each MB was obtained by calculating the ratio between the inflection point radius value obtained from the histogram MATLAB script data and the inflection point radius measured 2 d after production using Coulter Counter data. The accurate measurement of the inflection point was challenging for F1- and F2-MBs with 0 mol% PF due to their polydispersity. However, for F2-MB an approximation was made of the in chip-radius, considering the highest inflection point.

The shelf stability was evaluated by the obtained 5 time points from the Coulter counter measurements as a function of the normalized concentration for each MB. The monodispersity quantification at 2 d was evaluated by fitting the curves to the gaussian distribution to obtain the parameters σ and μ. Then, the coefficient of variation (CoV) was calculated using Eq 3 to evaluate the dispersity of the MB [89].

$$CoV = \sigma/\mu \qquad \text{Eq 3}$$

The size stability of each MB was quantified by obtaining the coefficient of variation (CV) as a percentage by the ratio of the standard deviation to the mean.

The stiffness (χ) of the MBs shell was obtain 2 d after production using Eq 4, which was obtained by solving Eq 2 in order to χ, with $\omega_0 = f_0\ 2\pi$.

$$\chi = \frac{R_0}{4}\left((\omega_0 R_0)^2 \rho L - (3\kappa \mathrm{P}_0) - (\,3\kappa - 1)\frac{2\sigma(R_0)}{R_0}\right) \qquad \text{Eq 4}$$

4 Results

4.1 Microbubble Production

Figure 17 provides an illustrative example of the bright-field images captured using high speeding imaging.

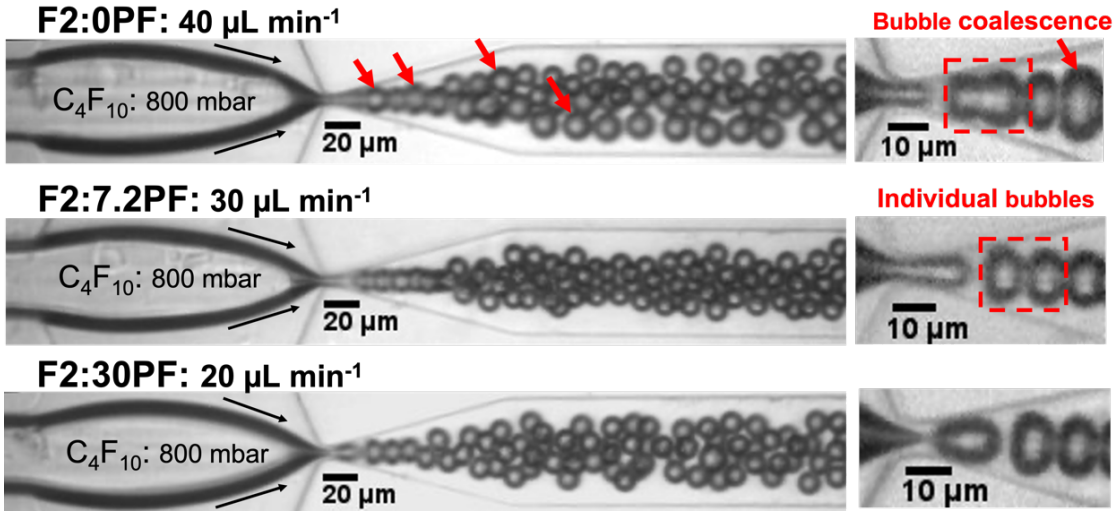

Figure 17 – Bright-field images showcase three examples of the production of MBs using a flow-focusing device at room temperature. A gas pressure of 800 mbar and varying liquid flow rates were used to achieve an on-chip radius around 6 µm. The images represent F2-MBs with 0, 7.2, and 30 mol% PF, arranged from top to bottom, respectively. The larger field-of-view pictures on the left were captured at a rate of 200 Kfps, while the zoomed-in images of the nozzle on the right were taken at a rate of 600 Kfps.

The presented images represent F2-MBs with 0, 7.2, and 30 mol% PF. Without PF, immediate coalescence was observed right after MB pinched off at the nozzle (top, right). In the outlet channel (top, left), the percentage of coalesced MBs was approximately 50% for F2:0PF-MB (examples of coalesce MBs indicated by red arrows). In contrast, the addition of PF prevented coalescence directly after the nozzle and in the outlet. Although not all images are presented here, a consistent pattern was observed across both formulations. F1- and F2-MBs without PF displayed immediate coalescence after the nozzle. However, when incorporating PF, coalescence-free monoMBs were successfully produced.

4.1.1 On-chip Size Distribution

The histograms showed in Figure 18 represent the on-chip radius distribution of each MB. It is important to note that due to the inconsistency in the number of recordings taken for each MB, the amount of measured MB is not consistent.

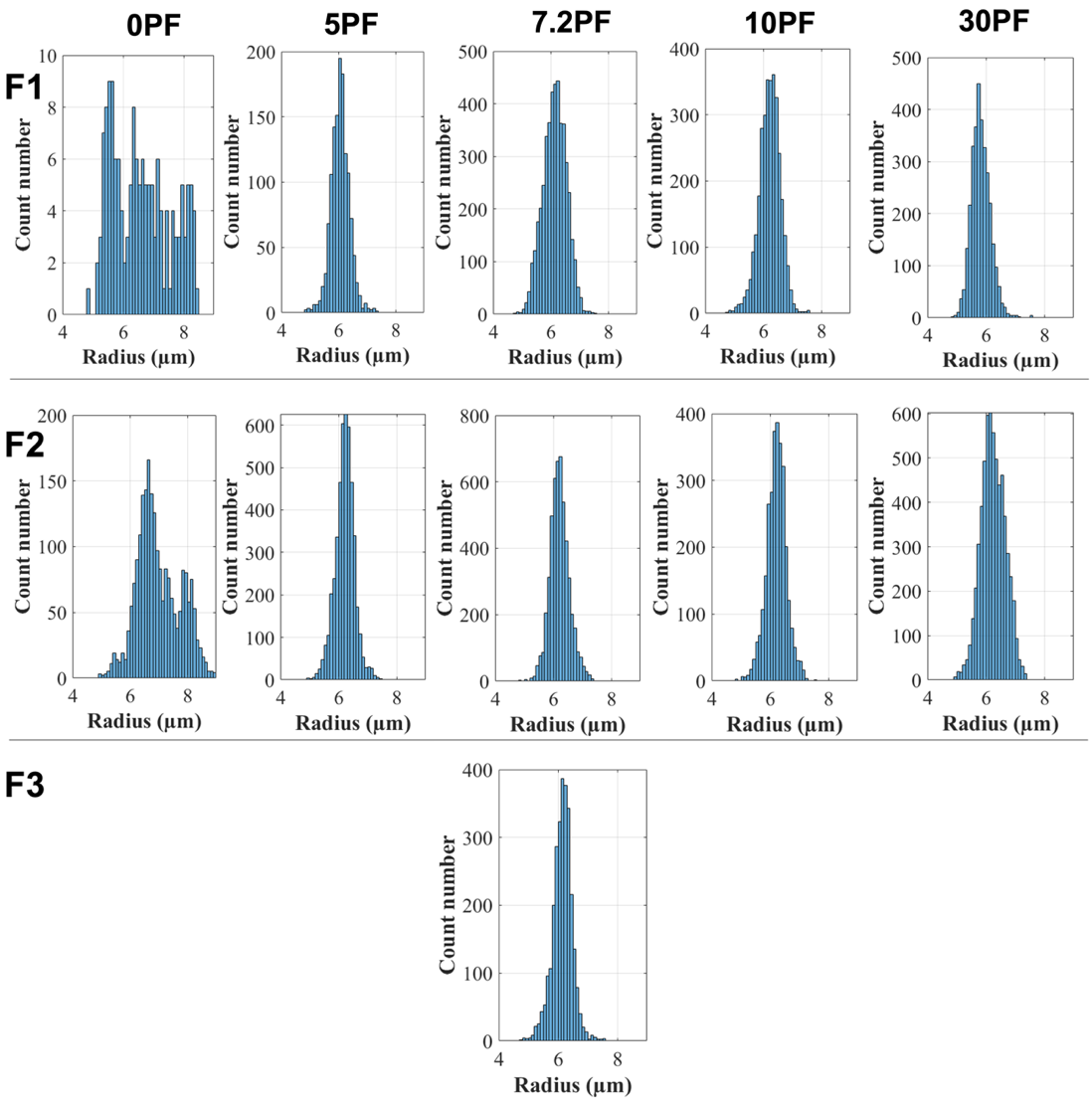

Figure 18 – Histograms of the on-chip size distribution of 11 MBs during production, with an on-chip radius around 6 µm. F1-MBs (top figures), F2-MBs (middle figures) at 0, 5, 7.2, 10, and 30 mol% PF, (left to the right) and F3-MB (bottom figure) at 7.2 mol% PF.

As can be seen from the Figure, 0 mol% PF resulted in MBs with a wide on-chip size distribution ranging from 5-9 µm with multiple inflection points, which represents coalescence happening. In contrast, MBs that incorporate 5, 7.2, 10, and 30 mol% PF displayed a single inflection point around 6 µm with a gaussian distribution, indicating the generation of non-coalescence monoMBs.

4.2 Shelf Stability

The shelf stability of the produced MBs was monitored over a period of 7 d, with measurements taken at 5 specific time points: 2 h, 1 d, 2 d, 4 d, and 7 d. The starting point, t=0, was defined as the moment when the collection of 1 mL of MBs in the sealed vial was concluded. The size distribution of the MBs is presented in Figure 19 for the two MBs produced without PF (F1:0PF-MB and F2:0PF-MB), and the two produced with 30 mol% PF (F1:30PF-MB and F2:30PF-MB).

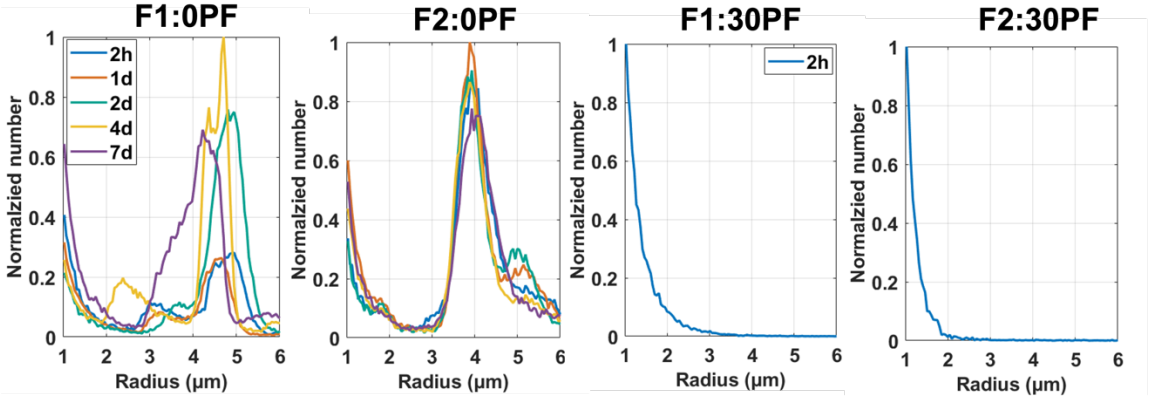

Figure 19 - Shelf stability. Size distribution and normalized concentration of 4 MBs. F1- and F2-0PF-MBs over 7 d (left figures). F1- and F2-30PF-MBs at 2 h (right figures).

F1:0PF-MB and F2:0PF-MB result in a polydisperse size distribution with multiple inflection points, where one peak had a significantly higher concentration than the other. F1:0PF-MB demonstrated low shelf stability throughout the 7 d in contrast to the F2:0PF-MB. F1:0PF-MB initially reached a radius of approximately 5 µm (higher concentration) and 3-4 µm (lower concentration) within 2 h, but experienced a leftward shift after 4 d, indicating size instability. Concentration variations were also observed, with a notable increase at 4 d followed by a decrease at 7 d, demonstrating concentration instability. On the other hand, F2:0PF-MB shrunk to a final radius of approximately 4 µm within 2 h and maintained stability in both size and concentration over the 7-d period. F1:30PF-MB and F2:30PF-MB dissipated after 2 h suggesting instability or undetectable presence of MBs.

Figure 20 illustrates the size distribution of the MBs produced using 5, 7.2, and 10 mol% PF for F1- and F2-MBs, and 7.2 mol% PF for F3-MB.

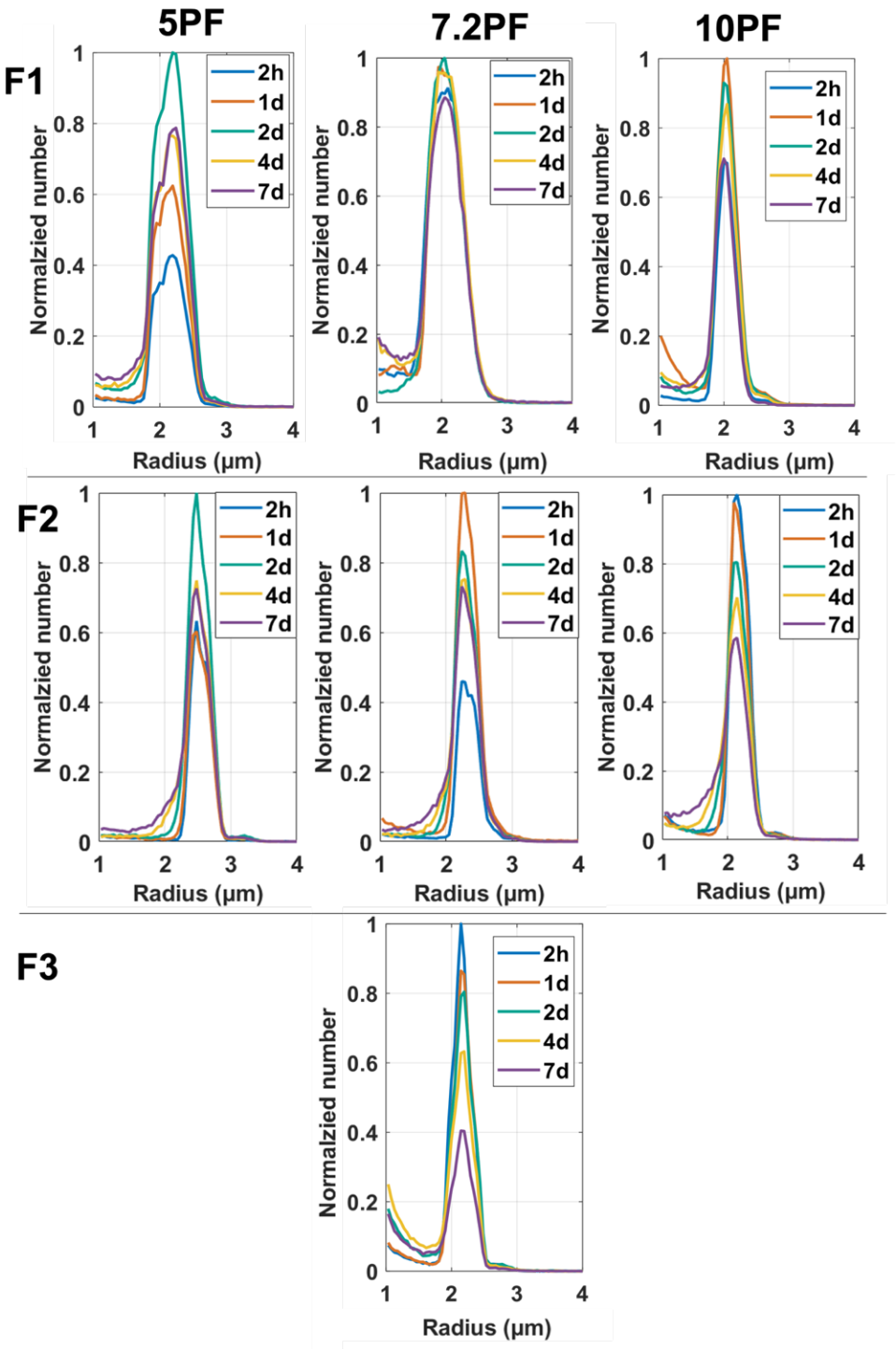

Figure 20 – Shelf stability size distribution over 7 d and normalized concentration of 7 MBs. F1-MBs (top figures), F2-MBs (middle figures) at 0, 5, 7.2, 10, and 30 mol% PF, (left to the right) and F3-MB (bottom figure) at 7.2 mol% PF.

The incorporation of 5, 7.2, and 10 mol% PF significantly improved the shelf stability of monoMBs. All MBs remained size-stable after shrinking to their final radius. The distribution curves displayed well-defined inflection points and a narrow size distribution

like a Gaussian curve. Nonetheless, F1:5PF-MB showed a slight deviation on the left side of the curve, while F1:7.2PF-MB exhibited a zigzag peak at 2 h and 4 d.

The MBs exhibited varying concentration stability patterns. Both F2:10PF-MB and F3:7.2PF-MB reached their highest concentration at 2 hours. F1:10PF-MB and F2:7.2PF-MB at 1 day, while F1:5PF-MB, F1:7.2PF-MB, and F2:5PF-MB at 2 days. F3:7.2PF-MB showed a continuous decrease in concentration over 7 d. When considering the highest concentration and the 7 d concentration, F3-MB exhibited the highest decrease (60%), followed by F2:10PF-MB (41%) and F1:10PF-MB (30%). F1:5PF-MB decreased by 22%, while F2:5PF-MB and F2:7.2PF-MB decreased both by 29%. The lowest decrease occurred to F1:7.2PF-MB (29%). These results indicate that F2 had lower concentration stability compared to F1. While F1- and F2-MBs with 5 and 7.2 mol% PF showed concentration stability between days 4 and 7, those with 10 mol% PF experienced a decrease in concentration during the same period.

In this study, photographs of the vials were taken 10 min after Coulter counter measurements to visually assess the shelf stability of the MBs. As an example, Figure 21 illustrates F1-MBs with 10, 30, and 0 mol% PF.

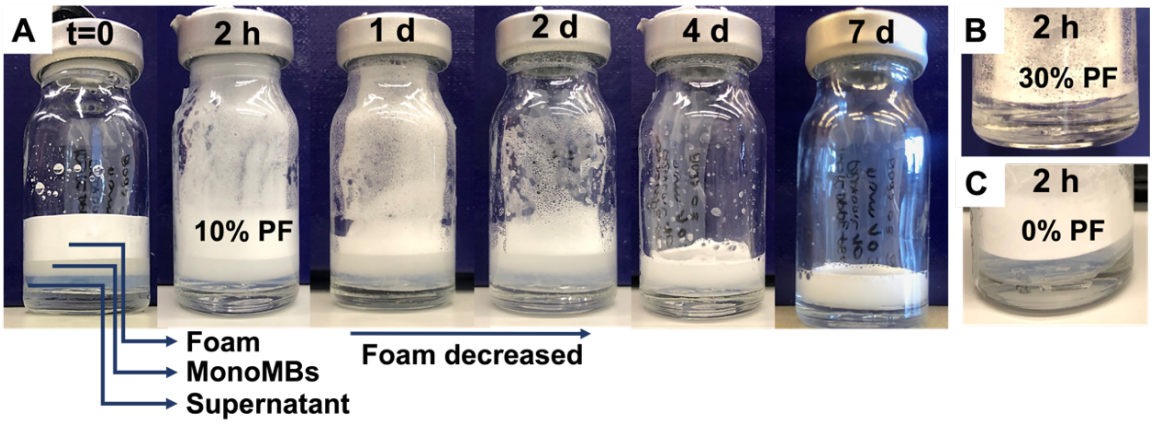

Figure 21 – F1-MBs observed inside a sealed vial filled with C_4F_{10} gas. A) Sequential images showcasing the stability of F1:10PF-MB over time, from t=0 (post-production) to 7 d. B) Image capturing the unstable state of F1:30PF-MB after 2 h. C) Image showing F1:0PF-MB 2 h post-production with a visible foam of MBs.

For F1:10PF-MB (Figure 21, A), sequential images were captured from t=0 (post-production) to 7 d. As can be observed, the foam layer gradually reduced, while the middle layer (monoMBs) increased in volume from t=0 to 1 d, indicating the occurrence of Ostwald Ripening phenomenon (dissolution of bigger MBs to reach a stable final size

of the monoMBs in the middle layer). These findings align with those observed for the same MB (Figure 20) where the increase in the concentration of monoMBs until day 4 corresponds to the reduction in foam observed until the same day. In contrast, the image (Figure 21, B), for F1:30PF-MB revealed the absence of both the foam layer and monoMBs layer after 2 h. Additionally, F1:0PF-MB (Figure 21, C), exhibited the presence of two top layers, indicating the existence of MBs after 2 h. These outcomes were consistent measured MBs in the Coulter counter (Figure 19).

The focus was primarily placed on the shelf stability where the concentration normalization was done to ensure a fairer comparison between the different MBs. However, it is equally important to demonstrate the disparities in between MBs (number of MB/mL) 2 d after production, as illustrated in Figure 22.

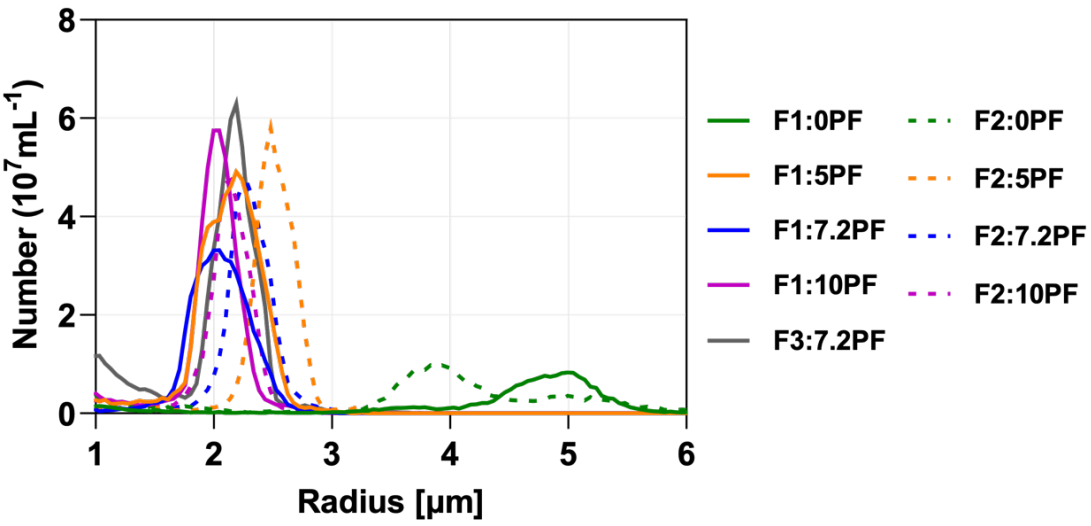

Figure 22 – Concentration of F1, F2, and F3-MBs 2 d after production.

The final concentration of the MBs without PF (shown by the green lines) was considerably lower due to the occurrence of coalescence, a phenomenon that leads to a broader size distribution among the MBs. In contrast, the monoMBs showed a higher concentration of MBs within the final stable size.

4.2.1 Monodispersity Quantification

The CoV was used to assess the monodispersity among MBs, where a lower CoV indicated a narrower distribution, and the results are presented in Table 2.

Table 2 –Monodispersity of MBs at 2 d quantified with CoV (%).

Formulation	mol% PF	Monodispersity (CoV %)
F1	5	11
	7.2	12
	10	7
F2	5	6
	7.2	7
	10	7
F3	7.2	8

According to the data presented in the table, the results indicate variations in monodispersity among different types of MBs. Specifically, F1:5PF-MB and F1:7.2PF-MB displayed relatively higher monodispersity at 2 d, as evidenced by CoV values of 11% and 12% respectively. Conversely, F1:10PF-MB exhibited a comparable level of monodispersity to the other MBs, with a CoV of 7%. Among the F2-MBs, similar monodispersity was observed, with 5, 7.2, and 10 mol% PF-MBs showing CoV values of 6%, 7%, and 7% respectively. F3:7.2PF-MB displayed a CoV value of 8%. When comparing F1, F2, and F3 with 7.2 mol% PF, it is noteworthy that F1 exhibited relatively lower monodispersity at 2 d.

4.2.2 Size Stability Quantification

Figure 23 shows the peak radius at each time point over 7 d for each MB.

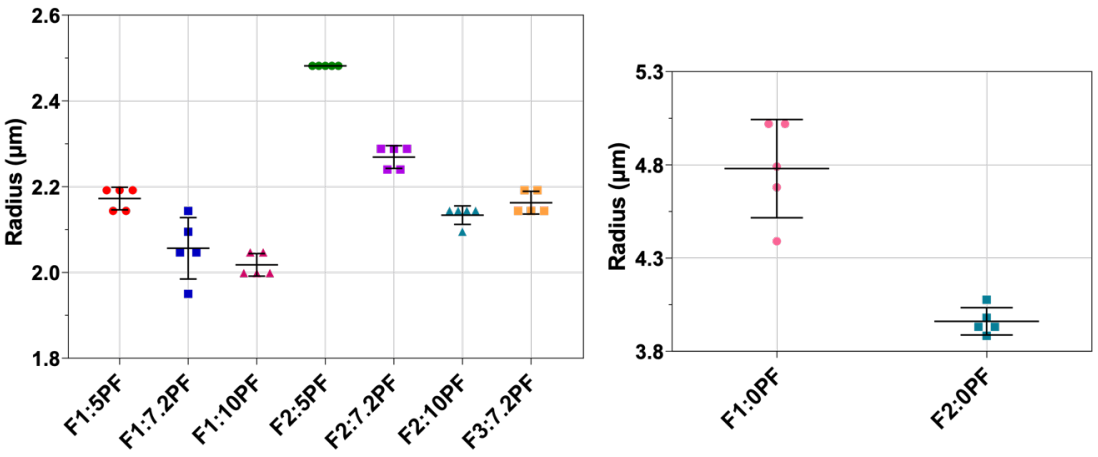

Figure 23 - Radius stability for the 7 MBs represented on the left figure (F1-and F2-MBs with 5, 7.2, and 10 PF, as well as F3-7.2PF) and for F1:0PF-MB and F2:0PF-MB on the right figure. Each symbol represents the measured radius over the 7 d. The overlaid black lines represent the mean and standard deviation of the measurements.

The left figure displays F1-MBs and F2-MBs with 5, 7.2, and 10 mol% PF, along with F3-MB with 7.2 mol% PF. The radius ranges from 1.95 µm to 2.48 µm. On the right figure, F1-MB and F2-MB with 0 mol% PF are shown, with a radius range of 3.88 µm to 5.02 µm.

To assess the size stability of the MBs more accurately, the coefficient of variation (CV) was calculated and is presented in Table 3.

Table 3 – Quantification of the size stability over 7 d by the coefficient of variation.

Formulation	mol% PF	Size stability (CV%)
F1	0	5.51
	5	1.22
	7.2	3.49
	10	1.31
F2	0	1.85
	5	0.00
	7.2	1.17
	10	1.01
F3	7.2	1.22

As shown in the table, for both formulations, 5 mol% PF exhibited lowest CV values, while 7.2 mol% PF showed highest CV values. Notably, all F2-MBs displayed lower CV values when compared to F1-MBs, suggesting superior size stability for the F2 formulation. Further examination of F1-MB, F2-MB, and F3-MB formulated with 7.2 mol% PF revealed that F1-MB exhibited the lowest size stability, with a CV of 3.49%, in contrast to F2-MBs (1.17%) and F3-MBs (1.22%). F2:0PF-MB exhibited a smaller radius and a lower CV of 1.85% when compared to F1:0PF-MB (5.51%). F2:0PF-MB demonstrated lower size dispersion (1.85%) over the 7 d period compared to F1:7.2PF-MB (3.49%).

4.3 Shrinkage Rate

To gain a deeper understanding of the impact of PF on the MB size, the shrinkage rate was calculated and is presented it in Table 4.

Table 4 - MB shrinkage rate, calculated as the ratio between the initial on-chip radius obtained from the highest value of the histogram size distribution, and the final stable radius obtained from the inflection point of the size distribution on the Coulter counter 2 d after production.

Formulation	mol% PF	On-chip radius (μm)	Final radius (μm)	Shrinkage rate (-)
F1	0	-	-	-
	5	6.05	2.16	2.80
	7.2	6.25	2.05	3.05
	10	6.35	2.04	3.11
	30	5.75	-	-
F2	0	6.65	3.9	1.60
	5	6.25	2.52	2.48
	7.2	6.25	2.30	2.72
	10	6.25	2.15	2.86
	30	6.16	-	-
F3	7.2	6.25	2.18	2.87

MBs with addition of 30 mol% PF could not be measured 2 h after production for both formulations. For the same formulation, MBs containing 10 mol% PF exhibited the smallest radius compared to the other mol% PF. F2:0PF-MB exhibited a smaller radius over 7 d compared to F1:0PF-MB. Analyzing F1- and F2-MBs with 5, 7.2, and 10 mol% PF, a consistent trend emerged where an increased mol% PF corresponded to higher shrinkage rate (F1: 2.80, 3.05, and 3.11; and F2: 2.48, 2.72, and 2.86, respectively). Moreover, for F2:0PF-MB, the shrinkage rate calculated by an approximated measurement was ∼1.60. This suggests that PF exerts an influence on the final size of the MBs, with higher mol% PF leading to a higher shrinkage rate and consequently a smaller final stable radius.

4.4 Attenuation Measurements

Figure 24 displays the attenuation spectra ranging from 1 to 5 MHz, measure at an acoustic pressure of 10 kPa, for F1-, and F2-MBs with 0, 5, 7.2, and 10 mol% PF.

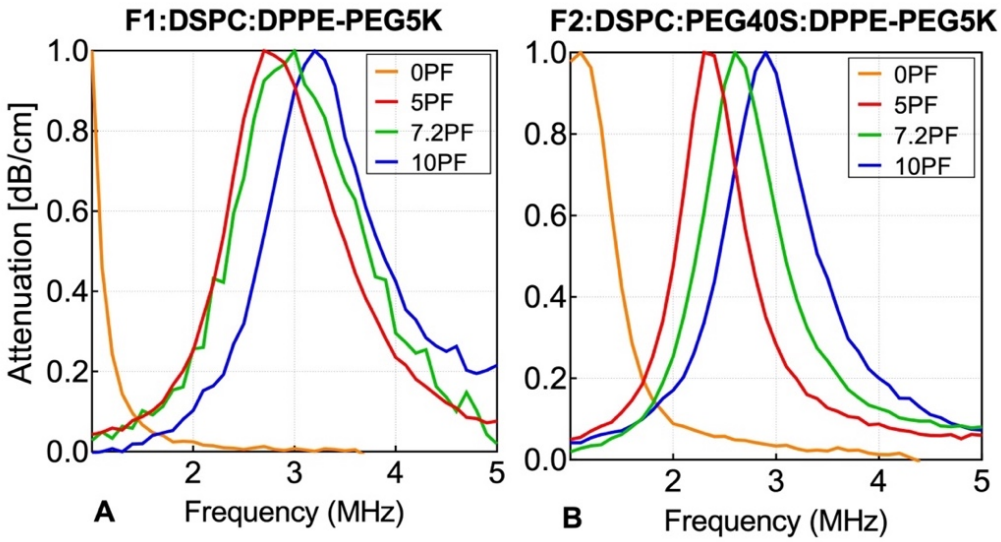

Figure 24 - Attenuation curves measured at an acoustic pressure of 10 kPa for 0, 5, 7.2, and 10 mol% PF. A) F1, and B) F2.

F1-, and F2-MBs exhibited similar acoustic responses. The formulations without PF, due to its higher radius, have a smaller resonance frequency. Therefore, they did not respond within the frequency range of 1-5 MHz (orange line). On the other hand, 5PF-MB, 7.2PF-MB, and 10PF-MB for F1 and F2 exhibited a consistent pattern, showing a peak response around 3 MHz with a slight shift towards higher frequencies as the mol% PF increased. In the case of F1, the peak attenuations for 5PF-MB, 7.2PF-MB, and 10PF-MB were at frequencies of 2.7, 3.0, and 3.2 MHz, respectively (Figure 24 A). Similarly, for F2, the peak attenuations for 5PF-MB, 7.2PF-MB, and 10PF-MB were at frequencies of 2.3, 2.6, and 2.9 MHz, respectively (Figure 24 B). The slight differences in the resonance frequencies can be attributed to the decrease in MB size that occurs with an increase in mol% PF or to differences in the stiffness of the shell. Additionally, it is noteworthy that the addition of PEG40S to F2 does not appear to have a significant impact on the resonance frequency.

Figure 25 shows the attenuation curves for F1, F2, and F3 with 7.2 mol% PF.

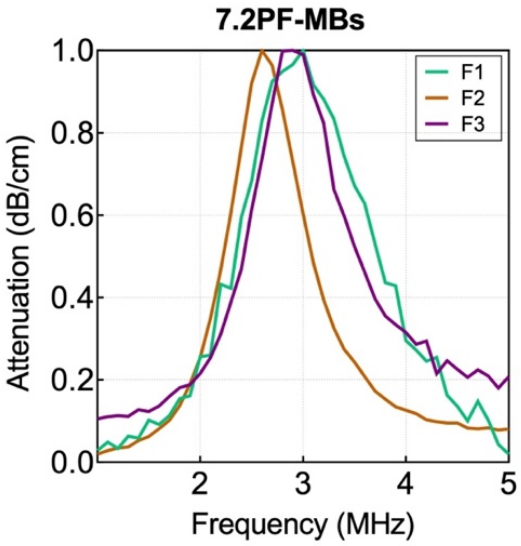

Figure 25- Attenuation curves measured at an acoustic pressure of 10 kPa for F1-, F2-, and F3-MBs with 7.2 mol% PF.

No discernible differences were observed among the three formulations. Both F1 and F3 displayed an attenuation peak around 3 MHz, while F2 exhibited a peak at 2.6 MHz. These results indicate that the presence of different surfactants in the shell, such as PEG40S in F2 and F3, and the substitution of DPPE-PEG5K with DSPE-PEG5k in F3, did not have any significant influence on resonance frequency of the MBs.

The shell stiffness of the MBs was obtained from the eigenfrequency of the attenuation curves, taking into consideration the MB radius in the inflection point at 2 d (Table 5).

Table 5- Stiffness of the shell obtained at t=2 d.

Formulation	mol% PF	Eigenfrequency (MHz)	Radius at 2 d (μm)	Stiffness (N/m)
F1	5	2.7	2.16	0.55
	7.2	3.0	2.05	0.60
	10	3.2	2.04	0.69
F2	5	2.3	2.52	0.63
	7.2	2.6	2.30	0.62
	10	2.9	2.15	0.65
F3	7.2	2.8	2.18	0.62

The stiffness values for all the MB formulations range from 0.55 to 0.69 N/m. When analyzing the effect of PF on the shell stiffness, it was observed that for F1, the stiffness

increased with the mol% PF. Specifically, F1:5PF-MB, F1:7.2PF-MB, and F1:10PF-MB had stiffness values of 0.55, 0.60, and 0.69 N/m, respectively. However, for F2, no clear relation between the mol% PF and the stiffness was observed. Comparing F1:7.2PF-MB (0.60 N/m), F2:7.2PF-MB (0.62 N/m), and F2:7.2PF-MB (0.62 N/m), it can be concluded that the stiffness was independent of the lipid formulation and the mol% PF. The higher difference in the stiffness for F1-MB with 5, and 7.2 mol% are more likely due to the broader size distribution observed for these two MBs. Furthermore, the addition of PEG40S for F2 or changing DPPE-PEG5k for DSPE-PEG5K did not have any effect on the stiffness.

4.5 Lower the Lipid Concentration

In the present study, the lipid concentration utilized for the MBs discussed above was 20 mg/mL. This higher lipid concentration was chosen to prevent coalescence and enhance stability of the MBs. However, it should be noted that this concentration is significantly higher (by a factor of 100) compared to the concentrations employed in commercially available polydisperse agents [1, 10].

To address the cost-effectiveness of the process, we investigated the feasibility of using PF as a substitute of lipid to prevent coalescence in low lipid concentration. By decreasing the lipid concentration by a factor of 4, we achieved a concentration of 5 mg/mL for the formulation F2 with 20% mol PF (referred to as 5 mg/mL-F2:20PF-MB). The production conditions for this MB were kept consistent with the ones described earlier, including an applied pressure of 800 mbar and an on-chip radius of approximately 6 µm. The results regarding the on-chip size distribution, shelf stability, and shrinkage rate are presented in Figure 26.

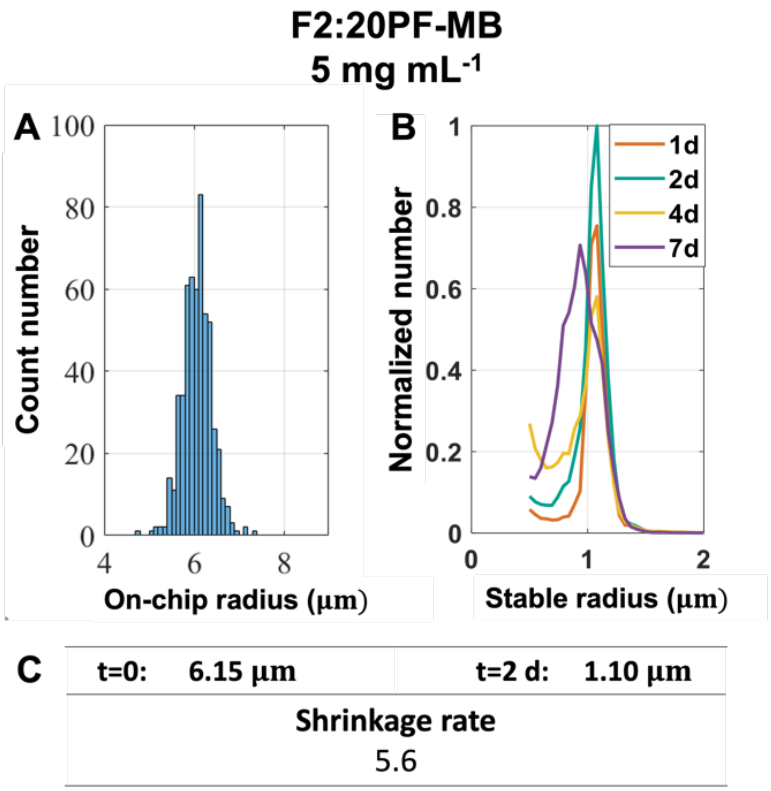

Figure 26 - Lower the lipid concentration to 5 mg/mL for F2-MB with 20 mol% PF (5 mg mL^{-1} F2:20PF-MB). A) On-chip size distribution. B) Shelf stability over 7 d. C) Shrinkage rate.

The 5 mg/mL-F2:20PF-MB was successfully produced without coalescence and exhibited a monodisperse size distribution on the chip (Figure 26, A). The shelf stability was assessed over a period of 7 d (Figure 26, B). The MB maintained its size stability until 4 d with a slight leftward shift at 7 d. In terms of concentration stability, this MB displayed a similar behavior to the above study MBs, with an initial increase in concentration at 2 d. The concentration stability appeared promising, as the same concentration observed at 1 d was maintained at 7 d. Furthermore, the shrinkage rate was calculated (Figure 26, C), and having a radius of 1.10 µm at 2 d, the resultant shrinkage rate was determined to be 5.6. This finding aligns with the observed trend in other MBs (Table 4), where a higher mol% PF led to higher shrinkage rates.

5 Discussion

PF added to the lipid solution, successfully resulted in the production of monoMBs in a MFFD, at room temperature, that were coalescence-free, stable for at least 7 d when produced with 5, 7.2, and 10 mol% PF, and acoustically responsive. Adding 30 mol% PF resulted in an unstable MB after 2 h. To the best of our knowledge, our work is the first that investigated the effects of PF on the shelf stability and acoustic properties of lipid monoMBs.

5.1 Coalescence

MBs produced without PF immediately coalesced in the outlet channel (Figure 17) leading to a broader size distribution i.e., polydisperse, with a final radius ranging from 4 to 5 µm (Figure 18). Consequently, 2 d after production, a reduced concentration of MBs at the desired size was observed (Figure 22). However, the addition of PF to the lipid solution at mol% of 5, 7.2, 10, and 30, successfully enabled the production of monoMBs at a gas pressure of 800 mbar and varying the flow rates, which was not possible without PF. As shown in Figure 17, the on-chip coalescence was effectively prevented, resulting in a uniform MB radius size distribution with a distinct inflection point around 6 µm (Figure 18). Moreover, during the stabilization process of these PF-MBs, coalescence did also not occur, leading to a monodisperse distribution after 2 h (Figure 20).

Previous studies have demonstrated the successful production of PF-monoMBs using FFMDs. In one study [15], 82.7 mol% PF was added to a lipid solution containing DSPC:DSPE-PEG2000 (similar to our F1, DSPC:DSPE-PEG5000), at the same concentration of 20 mg/mL. This high mol% PF suppressed coalescence; however, it is questionable whether the produced MBs were lipid- or polymer-coated, as 82.7 mol% of the shell consisted of PF. Another study [80], also incorporate PF into a protein (oleosin)-coated MB, resulting in the production of monoMBs with both high shelf and acoustic stability.

According to prior research, so only a small fraction (0.1%) of the total lipids present in the solution are responsible for forming a coating on the MBs in a FFMD [50]. The remaining lipids form liposomes within the thin liquid film between newly formed MBs

[12]. The presence of these liposomes (mainly PEGylated vesicles [32]) increases the apparent viscosity of the thin film and generates additional repulsive steric surface that interact with the PEGylates molecules around the MBs, reducing the probability of coalescence [13]. Our assumption is that the surfactant PF replace the role of liposomes, by spontaneously assembles into micelles when its concentration exceeds the critical micelle concentration (cmc). This offers a significant advantage since PF is as a cost-effective alternative to the typically expensive lipids used for coating MBs. We hypothesize that there are two primary benefits through the incorporation of PF Firstly, it helps prevent coalescence of the MBs, and secondly, lower the amount of emulsifiers in the shell is expected to result in higher resonance frequency and stiffer shell [14]. This final assumption was based in an experimental observation where the shell stiffness had a significant increase from 0.8 to 2.5 N/m with the number of insonations due to the loss of DSPE-PEG5000, i.e., higher acoustic response with slightly less emulsifier in the shell [14].

5.2 Shelf Stability

The above mentioned study [15] lacked shelf stability evaluation when 82.7 mol% PF was incorporated into the MB formulation. Here, we observed that for F1, the addition of 5, 7.2, and 10 mol% PF resulted in significant improvements in shelf stability (Figure 20) including concentration stability, size stability, and monodispersity, when compared to the formulation without PF (Figure 19). In contrast, for formulation F2, although PF had a positive effect in suppressing coalescence and achieving a narrower size distribution, no clear correlation was observed between concentration and size stability. Comparing F2 and F3 both with 7.2 mol% PF, the change from DPPE-PEG5000 to DSPE-PEG5000 led to a decrease in concentration stability, while no significant differences were observed in terms of monodispersity and size stability.

We also aimed to compare the shelf stability of F1 with F2 (DSPC:PEG40S:DPPE-PEG5000), as PEG40S was reported to improve shelf stability [54]. Indeed, it was observed that without PF, PEG40S significantly increased the shelf stability of F2:0PF-MB compared to F1:0PF-MB. Other study suggested that PEG40S possibly enhances MB formation [90], thereby playing a role in the initial coating of the shell, and consequently, improving MB

stability. Additionally, the same study suggested that a portion of PEG40S during stabilization can be excluded from the coating into the solution, for MBs with diameters under 2 µm. In terms of concentration, no significant differences were observed between F1-MBs and F2-MBs, possibly because PF alone is sufficient to achieve concentration stability. Moreover, CV obtained to quantify size stability, indicated that F2-MBs were the most size-stable. However, this could be attributed to the presence of PEG40S or the differences in size of F2-MBs compared to F1-MBs. Furthermore, F2:5PF-MB demonstrated the highest size stability with a CV of 0%, suggesting that the combination of F2 with 5 mol% PF resulted in the most size-stable formulation.

Although the 10PF-MBs showed a decrease in concentration from 4 d to 7 d, suggesting a negative impact of the 10 mol% PF on concentration stability, the 20PF-MBs, increased in concentration in the same period. Overall, no clear relationship between the mol% PF and concentration stability was observed. The differences in concentration observed over the 7 d period are most likely due to the Ostwald ripening process that is probable random and influences the concentration over time. However, all the MBs with 5, 7.2, and 10 mol% PF would be stable enough for further medical applications.

F1:7.2PF-MB had the worst size stability with a CV of 3.49 and the lowest monodispersity with a CoV of 12%. However, they exhibited the highest concentration stability, with a minimal decrease of 11%. Additionally, F1:5PF-MB showed similar monodispersity has F1:7.2PF-MB with a CoV of 11%., while no significant differences were observed among the others (6% - 8%). These variations in monodispersity could be attributed to uncontrollable flow-rate fluctuations during production, resulting in size variations and a less monodisperse population. Manual adjustments were made to compensate for these fluctuations as we got more experience during the project months, but inherent limitations led to slight differences between MB batches.

As discussed earlier, no conclusions can be drawn about the shelf stability of F1 and F2 with 30 mol% PF, either because they are unstable and completely dissolve or because the Coulter counter is not sensitive to particles smaller than 1 µm. However, the literature strongly suggests that these MBs are not stable. A study [91] reviewed the literature and showed that for MBs to be stable, the primary lipid (DPSC) needs to constitute at least 70% of the shell to maintain coating integrity. In our study, to incorporate 30 mol% PF, the DSPC fraction needed to decrease to 63 mol% for F1 and 57.5 mol% for F2. This can

explain why these MBs were not stable, indicating that it was not directly due to the higher mol% PF, but rather the consequent decrease in the mol% of DSPC.

Lower the lipid concentration by a factor of 4 to 5 mg/mL using 20 mol% PF, result in monoMBs stable in size and concentration, with only instability in size observed at 7 d. However, this presents no significant problem, as the time window of 2 to 4 d provides ample duration suitable for direct *in vivo* injection [12].

5.3 Shrinkage rate

All monoMBs produced with 5, 7.2, and 10 mol% PF exhibited a consistent trend of dissolving to stable final radii ranging from 2.48 to 3.05 times smaller than their initial radii after 2 d. The increase in mol% PF corresponded to higher shrinkage rates, as shown in Table 4. An approximation value of the inflection point for the polydisperse on-chip size distribution for F2:0PF-MB was performed, resulting in a MB final radius ∼1.60 smaller. Furthermore, when 20 mol% PF was added to 5 mg/mL-F2:20PF-MB, a size reduction of 5.6 times to a final radius of 1.10 µm was observed (Figure 26). These results indicate that the PF content in MBs affects their final size, with higher mol% PF leading to a higher shrinkage rate.

The reduction in size and subsequent stabilization of the produced monoMBs after 2 h was expected due to the inherent instability of freshly produced MBs caused by Laplace pressure [40]. Previous studies have reported a stabilization time of 2 h for the majority of MBs [14], while others suggest 1 h is sufficient for MBs to stabilize [12]. Our shrinkage rate values are within the reported ranges obtained for monoMBs produced by FFMDs [12-14, 92]. While the shrinkage rate is independent of nozzle size and shear rate [14], as well as bulk viscosity and lipid concentration [13], it is sensitive to the lipid formulation [12, 13, 91]. Due to instability and polydispersity, we were unable to directly measure the shrinkage rate of F1:0PF-MB. However, for the F1:0PF-MB formulation, others have reported a shrinkage rate of 2.2 [37] when producing monoMBs at 55 °C. Consequently, a consistent trend emerged in which an increase in mol% PF (0, 5, 7.2, and 10) for F1-MB and (0, 5, 7.2, 10, and 20) for F2-MB resulted in increase in the shrinkage rate (∼2.2, 2.80, 3.05, and 3.11) and (∼1.60, 2.48, 2.72, 2.86, and 5.6), respectively.

An unexpected finding was observed for F1:30PF-MB and F2:30PF-MB after 2 h, demonstrating the absence or undetectable presence of MBs when higher mol% PF was incorporated. We hypothesize that the shrinkage rate for these 30PF-MBs is too high, consequently the final radius of the bubbles is near 0 µm or at the nanoscale. This means that either the MBs were not detected by the Coulter counter, or the MBs were unstable and prone to complete dissolution due to their small size. In fact, the 5 mg/mL-F2:20PF-MB demonstrated instability in both size and concentration after 7 d, possibly due to their smaller size (1.10 µm) compared to the stable monoMBs produced with radii of 2-3 µm. Previous literature reported that smaller air MBs (5, 3, and 1 µm) dissolved in 90, 25, and 2 ms, respectively [9]. While the coating of our MBs significantly improves their life-time, a small radius will invariably lead to high surface tension and inherent instability [56, 57].

The tip streaming mechanism, proposed by Shelley and Hans [55], gives an explanation for the formation MBs in a MFFD, where the elongational flow induces the surfactants to adsorb at different gradients along the liquid/gas interface, leading to a highly curved tip densely packed with surfactants. When the shear forces near the interface break the lipid micelles, PF micelles and the micelles with a mixture of both surfactants in the liquid phase, we expected that lipid and PF molecules are adsorbed in their respective mol% ratio. According to literature [14], the residence time (τ_r) of the surfactant in the shell can be estimated by the equation Eq 5:

$$\tau_r = 55\tau_0/\mathrm{cmc} \qquad \text{Eq 5}$$

where $\tau_0 = 10^{-7}$. PF has a significantly lower cmc (3.8 x 10^{-5} M [93]) compared to DSPC (5 x 10^{-10} M [94]). With the mentioned cmc for PF and DSPC it is possible to estimate the residence time of DSPC lipid, ~3 h, in contrast to the much shorter residence time of PF, ~0.14 s. Therefore, it is expected that the number of lipid molecules in the bubble shell remains unchanged, while the PF is mostly or entirely expelled. By the literature it is well-known, that during the 2 h of stabilization the lipids remain in the shell [12], and it was also suggested that PF could indeed escape from the shell after MB formation [78, 81]. Consequently, when the tip is drawn into a thin thread and breaks into individual MBs, the shell is momentarily coated with lipids and PF, but the PF quickly escapes, creating open spaces on the shell surface. Increasing the mol% PF leads to more initial PF adsorption during MB formation, but the subsequent escape results in more free spaces

and consequently, a higher shrinkage rate to achieve the same fully packed lipid configuration.

5.4 Shell Stiffness

MonoMBs formed with PF demonstrated acoustic responsiveness at 10 kPa, as shown in Figure 24 and Figure 25. The resonance frequency predominantly occurred at 3 MHz, with slight shifts to higher frequencies as the mol% of PF increased, likely due to smaller MB sizes. However, it is important to note that increasing the stiffness of the shell can also affect the resonance frequency. In our study, we did not observe a significant effect of PF on the shell stiffness (Table 5). The monoMBs stiffness ranged from 0.55 to 0.69 N/m. The outlier observed for F1:5PF-MB, with a stiffness of 0.55 N/m is more likely due to the less well-defined inflection point in the curve at 2 d, along with a broader size distribution. This makes the measurement of shell stiffness less accurate, as the used equation it only considers MBs with one size at the inflection point. Furthermore, the addition of PEG40S did not change the shell stiffness significantly, possibly because, only a small portion remains in the shell after stabilization. The closest comparison found was with MBs coated with DPPC:DPPE-PEG5000, which had similar sizes ranging from 2.0 µm to 2.7 µm and a stiffness of 0.6 N/m [107]. However, it is important to note that this comparison may not be fair due to different setups and equation used for measuring attenuation and stiffness, respectively. We hypothesize that although no changes in stiffness were observed when testing MBs with 5 to 10 mol% PF, PF is likely to influence the stiffness of the MBs when compared to 0PF-MBs. This assumption is based on a study using MBs coated with oleosin, which showed that increasing the concentration of PF resulted in increased stiffness of the MBs [80].

5.5 Limitations of the Study

The main limitation found in this study relates to the Horizon bubble maker system itself, specifically the fluctuating liquid flow rate over time. The liquid pumps use feedback control, and then temperature sensor is used to calculate the flow speed, assuming the solution is water. However, since we used a lipid solution, different particles within the

solution heat differently, resulting in fluctuations in the flow rate. As a result, even though we aimed to set just a specific flow rate, these fluctuations led to the formation of MBs with slightly varying sizes depending on the specific flow rate at the specific production moment. Consequently, the on-chip distribution of MBs was not completely monodisperse, with sizes ranging from approximately 4-7 µm.

Another limitation is associated with the microfluidic chip and the 0.5 µm filter used to prevent the injection of dust or larger particles into the microfluidic channels. We found several blockages of the nozzle during production, mainly when we applied higher pressures, that caused particles to pass through the filter. This significantly increase the time required to produce a single batch of MBs, leaving us with insufficient time to repeat the experiments and test the reproducibility of the results.

6 Conclusions and Future Prospects

This work focused on the production of phospholipid-coated monoMBs at room temperature using a FFMD. The overall objective was to investigate the impact of PF on the coalescence and shelf stability of monoMBs, and also confirm their acoustic responsiveness. MonoMBs, as a type of UCA, are being extensively researched due to their potential to enhanced acoustic sensitivity with advantages for US imaging and drug delivery applications.

The coalescence of phospholipid-coated MBs can be suppressed by incorporating PF into the lipid solution with a lipid concentration of 20 mg/mL. This effect was observed in a flow-focusing device at room temperature, using gas pressure of 800 mbar and by changing the liquid flow rate to achieve an on-chip radius of 6 µm. Stable MBs were obtained by the addition of 5, 7.2, or 10 mol% PF. These MBs were stable for at least 7 d, with final radii ranging from 2.04 to 2.52 µm. However, it is crucial to carefully choose the percentage of PF because although 30 mol% PF prevented on-chip coalescence, the monoMBs dissolved after 2 h, most likely due to shell instability. By contrast, the incorporation of 20 mol% PF in a 5 mg/mL lipid formulation suppressed coalescence and resulted in stable MBs over 4 d with a final radius of 1.10 µm.

PF also to influence the final size of the monoMBs. Increasing the mol% PF led to a higher shrinkage rate, resulting in smaller monoMBs. This phenomenon is assume by us to happen because of the presence of open areas created when some PF escapes from the lipid shell. As a result, the MBs need to shrink more to achieve the same lipid packing. However, to determine if PF remains in the shell after stabilization, it will be necessary to label PF with a fluorescent marker.

The MB with the best performance was the F2:5PF-MB with the highest final radius of 2.52 µm along with no variation in size over the 7 d. The shelf stability of F1-MBs, was found to be a function of PF regarding F1:0PF-MB that was not stable at all. In contrast, F2:0PF-MB was stable in size and concentration, with the only difference between the formulation being the incorporation of PEG40S. In the last mentioned MB no improvements in the shelf stability were observed by adding PF. Therefore, we can concluded that PEG40S plays a significant role in stabilizing the freshly formed MBs.

Additionally, the increase in PF from 5 to 10 mol% did not have an effect on shelf stability in both formulations.

Different lipid coatings were also studied, specifically DSPC:DPPE-PEG5000 (F1), DSPC:PEG40S:DPPE-PEG5000 (F2), and DSPC:PEG40S:DSPE-PEG5000 (F3). F3:7.2PF-MB was found to be less stable in concentration over the 7 d compared to F1 and F2 with the same mol% PF. To take more conclusions about whether the emulsifier DPPE:PEG5000 provides better stability than DSPE-PEG5000, more experiments need to be done to assess the repeatability of the results.

The final aim of this study was to test if the monoMBs produced were acoustically responsive and to observe the effect of PF on the shell stiffness. The monoMBs had a resonance peak around 3 MHz, with a minimal increased frequency for smaller MBs. The mol% PF variation did not alter the shell stiffness, which was measured to range from 0.60 to 0.69 N/m.

The main question that remained to answer, is if PF is in the shell after stabilization, and how PF change the shell conformation. Therefore, the next step is to fluorescence the PF and observed with fluoresce microscopy if it is on the shell or not. Additionally, 4Pi confocal microscopy on a 0PF-MB and on the PF-MB will help us to compare the microstructure of the shells (LE and LC phases area) to see if PF changes its microstructure. Furthermore, to test if PF is in the shell and change elastic properties of it, it will be important to make an acoustic setup able to measure the bigger polydisperse MBs obtained without PF. This will allow us to investigate the the acoustic properties and behavior of these MBs, giving us useful information for comparison with the PF-coated MBs.

7 References

1. Helbert, A., et al., *Monodisperse versus Polydisperse Ultrasound Contrast Agents: In Vivo Sensitivity and safety in Rat and Pig.* Ultrasound Med Biol, 2020. **46**(12): p. 3339-3352.
2. Cosgrove, D., *Ultrasound contrast agents: an overview.* European Journal of Radiology, 2006. **60**(3): p. 324-330.
3. Versluis, M., et al., *Ultrasound Contrast Agent Modeling: A Review.* Ultrasound Med Biol, 2020. **46**(9): p. 2117-2144.
4. Chong, W.K., V. Papadopoulou, and P.A. Dayton, *Imaging with ultrasound contrast agents: current status and future.* Abdominal Radiology, 2018. **43**: p. 762-772.
5. De Jong, N., et al., *Principles and recent developments in ultrasound contrast agents.* Ultrasonics, 1991. **29**(4): p. 324-330.
6. Koczera, P., et al., *PBCA-based polymeric microbubbles for molecular imaging and drug delivery.* Journal of Controlled Release, 2017. **259**: p. 128-135.
7. Stride, E. and N. Saffari, *Microbubble ultrasound contrast agents: a review.* Proceedings of the Institution of Mechanical Engineers, Part H: Journal of Engineering in Medicine, 2003. **217**(6): p. 429-447.
8. Frinking, P., et al., *Three decades of ultrasound contrast agents: a review of the past, present and future improvements.* Ultrasound in Medicine & Biology, 2020. **46**(4): p. 892-908.
9. Segers, T., *Monodisperse bubbles and droplets for medical applications*. 2015: University of Twente. p. 187.
10. Stride, E., et al., *Microbubble Agents: New Directions.* Ultrasound in Medicine & Biology, 2020. **46**(6): p. 1326-1343.
11. Xie, Y., et al., *Closed-loop feedback control of microbubble diameter from a flow-focusing microfluidic device.* Biomicrofluidics, 2020. **14**(3): p. 034101.
12. Segers, T., et al., *Improved coalescence stability of monodisperse phospholipid-coated microbubbles formed by flow-focusing at elevated temperatures.* Lab on a Chip, 2019. **19**(1): p. 158-167.
13. Segers, T., et al., *Universal Equations for the Coalescence Probability and Long-Term Size Stability of Phospholipid-Coated Monodisperse Microbubbles Formed by Flow Focusing.* Langmuir, 2017. **33**(39): p. 10329-10339.
14. Segers, T., et al., *Stability of Monodisperse Phospholipid-Coated Microbubbles Formed by Flow-Focusing at High Production Rates.* Langmuir, 2016. **32**(16): p. 3937-3944.
15. Shih, R., et al., *Flow-focusing regimes for accelerated production of monodisperse drug-loadable microbubbles toward clinical-scale applications.* Lab on a Chip, 2013. **13**(24): p. 4816.
16. Feinstein, S.B., et al., *Two-dimensional contrast echocardiography. I. In vitro development and quantitative analysis of echo contrast agents.* Journal of the American College of Cardiology, 1984. **3**(1): p. 14-20.
17. Rudakovskaya, P.G., et al., *Microbubbles Stabilized by Protein Shell: From Pioneering Ultrasound Contrast Agents to Advanced Theranostic Systems.* Pharmaceutics, 2022. **14**(6): p. 1236.
18. Greis, C., *Ultrasound contrast agents as markers of vascularity and microcirculation.* Clinical Hemorheology and Microcirculation, 2009. **43**(1-2): p. 1-9.
19. Malone, C.D., et al., *Contrast-enhanced US for the interventional radiologist: current and emerging applications.* Radiographics, 2020. **40**(2): p. 562-588.
20. Kwan, J.J., et al., *Theranostic oxygen delivery using ultrasound and microbubbles.* Theranostics, 2012. **2**(12): p. 1174.
21. Fan, Z., R.E. Kumon, and C.X. Deng, *Mechanisms of microbubble-facilitated sonoporation for drug and gene delivery.* Ther Deliv, 2014. **5**(4): p. 467-86.

22. Khan, A.H. and S.V. Dalvi, *Kinetics of albumin microbubble dissolution in aqueous media.* Soft Matter, 2020. **16**(8): p. 2149-2163.
23. Abou-Saleh, R.H., et al., *Freeze-Dried Therapeutic Microbubbles: Stability and Gas Exchange.* ACS Applied Bio Materials, 2020. **3**(11): p. 7840-7848.
24. Sirsi, S.R. and M.A. Borden, *State-of-the-art materials for ultrasound-triggered drug delivery.* Advanced Drug Delivery Reviews, 2014. **72**: p. 3-14.
25. Sirsi, S. and M. Borden, *Microbubble Compositions, Properties and Biomedical Applications.* Bubble Sci Eng Technol, 2009. **1**(1-2): p. 3-17.
26. Hou, Z., et al., *Preparation and in vitro evaluation of an ultrasound-triggered drug delivery system: 10-Hydroxycamptothecin loaded PLA microbubbles.* Ultrasonics, 2012. **52**(7): p. 836-841.
27. Cesur, S., et al., *Metformin-loaded polymer-based microbubbles/nanoparticles generated for the treatment of type 2 diabetes mellitus.* Langmuir, 2021. **38**(17): p. 5040-5051.
28. Van Hoogevest, P. and A. Wendel, *The use of natural and synthetic phospholipids as pharmaceutical excipients.* European Journal of Lipid Science and Technology, 2014. **116**(9): p. 1088-1107.
29. Li, J., et al., *A review on phospholipids and their main applications in drug delivery systems.* Asian Journal of Pharmaceutical Sciences, 2015. **10**(2): p. 81-98.
30. Langeveld, S.A.G., *Microstructures in Theranostic Microbubbles*. 2022: Erasmus University Rotterdam. p. 305.
31. Pulsipher, K.W., et al., *Engineering Theranostic Microbubbles Using Microfluidics for Ultrasound Imaging and Therapy: A Review.* Ultrasound in Medicine & Biology, 2018. **44**(12): p. 2441-2460.
32. Segers, T., et al., *Foam-free monodisperse lipid-coated ultrasound contrast agent synthesis by flow-focusing through multi-gas-component microbubble stabilization.* Applied Physics Letters, 2020. **116**(17).
33. Borden, M.A., et al., *Lateral phase separation in lipids-coated microbubbles.* Langmuir. **22**(9): p. 4291-4297.
34. Borden, M.A., et al., *Surface phase behavior and microstructure of lipid/PEG-emulsifier monolayer-coated microbubbles.* Colloids Surf B Biointerfaces, 2004. **35**(3-4): p. 209-23.
35. Jugniot, N., et al., *Current status of targeted microbubbles in diagnostic molecular imaging of pancreatic cancer.* Bioengineering & Translational Medicine, 2021. **6**(1): p. e10183.
36. Kwan, J.J. and M.A. Borden, *Microbubble dissolution in a multigas environment.* Langmuir, 2010. **26**(9): p. 6542-6548.
37. Swanson, E.J., et al., *Phospholipid-stabilized microbubble foam for injectable oxygen delivery.* Langmuir, 2010. **26**(20): p. 15726-15729.
38. Gnyawali, V., et al., *Honey, I shrunk the bubbles: microfluidic vacuum shrinkage of lipid-stabilized microbubbles.* Soft Matter, 2017. **13**(22): p. 4011-4016.
39. Talu, E., et al., *Maintaining Monodispersity in a Microbubble Population Formed by Flow-Focusing.* Langmuir, 2008. **24**(5): p. 1745-1749.
40. Kilic, S. and E.S. Bolukcu, *Phase behavior of DSPC/PEG(40)St mixtures at higher emulsifier contents.* Colloids Surf B Biointerfaces, 2018. **171**: p. 368-376.
41. Segers, T., et al., *Monodisperse Versus Polydisperse Ultrasound Contrast Agents: Non-Linear Response, Sensitivity, and Deep Tissue Imaging Potential.* Ultrasound in Medicine & Biology, 2018. **44**(7): p. 1482-1492.
42. Talu, E., et al., *Tailoring the size distribution of ultrasound contrast agents: possible method for improving sensitivity in molecular imaging.* Molecular Imaging, 2007. **6**(6): p. 7290.2007. 00034.
43. Emmer, M., et al., *Pressure-dependent attenuation and scattering of phospholipid-coated microbubbles at low acoustic pressures.* Ultrasound Med Biol, 2009. **35**(1): p. 102-11.

44. Segers, T. and M. Versluis, *Acoustic bubble sorting for ultrasound contrast agent enrichment.* Lab Chip, 2014. **14**(10): p. 1705-14.
45. Kok, M.P., T. Segers, and M. Versluis, *Bubble sorting in pinched microchannels for ultrasound contrast agent enrichment.* Lab Chip, 2015. **15**(18): p. 3716-22.
46. Goertz, D.E., N. de Jong, and A.F. van der Steen, *Attenuation and size distribution measurements of Definity™ and manipulated Definity™ populations.* Ultrasound in Medicine & Biology, 2007. **33**(9): p. 1376-1388.
47. Feshitan, J.A., et al., *Microbubble size isolation by differential centrifugation.* Journal of Colloid and Interface Science, 2009. **329**(2): p. 316-324.
48. Yamada, M., M. Nakashima, and M. Seki, *Pinched flow fractionation: continuous size separation of particles utilizing a laminar flow profile in a pinched microchannel.* Analytical Chemistry, 2004. **76**(18): p. 5465-5471.
49. Langeveld, S.A., et al., *The impact of lipid handling and phase distribution on the acoustic behavior of microbubbles.* Pharmaceutics, 2021. **13**(1): p. 119.
50. Segers, T., N. de Jong, and M. Versluis, *Uniform scattering and attenuation of acoustically sorted ultrasound contrast agents: Modeling and experiments.* J Acoust Soc Am, 2016. **140**(4): p. 2506.
51. Xu, S., et al., *Generation of monodisperse particles by using microfluidics: control over size, shape, and composition.* Angewandte Chemie, 2005. **117**(5): p. 734-738.
52. Thorsen, T., et al., *Dynamic pattern formation in a vesicle-generating microfluidic device.* Physical Review Letters, 2001. **86**(18): p. 4163.
53. Anna, S.L., N. Bontoux, and H.A. Stone, *Formation of dispersions using "flow focusing" in microchannels.* Applied Physics Letters, 2003. **82**(3): p. 364-366.
54. Talu, E., et al., *Long-term stability by lipid coating monodisperse microbubbles formed by a flow-focusing device.* Langmuir, 2006. **22**(23): p. 9487-90.
55. Anna, S.L. and H.C. Mayer, *Microscale tipstreaming in a microfluidic flow focusing device.* Physics of Fluids, 2006. **18**(12): p. 121512.
56. Hall, R.L., et al., *Formulation and characterization of chemically cross-linked microbubble clusters.* Langmuir, 2019. **35**(33): p. 10977-10986.
57. Jamburidze, A., et al., *Nanoparticle-Coated Microbubbles for Combined Ultrasound Imaging and Drug Delivery.* Langmuir, 2019. **35**(31): p. 10087-10096.
58. Pu, G., M.A. Borden, and M.L. Longo, *Collapse and shedding transitions in binary lipid monolayers coating microbubbles.* Langmuir, 2006. **22**(7): p. 2993-2999.
59. Duncan, P.B. and D. Needham, *Test of the Epstein− Plesset Model for gas microparticle dissolution in aqueous media: effect of surface tension and gas undersaturation in solution.* Langmuir, 2004. **20**(7): p. 2567-2578.
60. Borden, M.A. and M.L. Longo, *Dissolution behavior of lipid monolayer-coated, air-filled microbubbles: Effect of lipid hydrophobic chain length.* Langmuir, 2002. **18**(24): p. 9225-9233.
61. Allen, C., et al., *Controlling the physical behavior and biological performance of liposome formulations through use of surface grafted poly (ethylene glycol).* Bioscience Reports, 2002. **22**: p. 225-250.
62. Abedi Karjiban, R., et al., *A coarse-grained molecular dynamics study of DLPC, DMPC, DPPC, and DSPC mixtures in aqueous solution.* Journal of Chemistry, 2013. **2013**.
63. Angile, F.E., et al., *Recombinant protein-stabilized monodisperse microbubbles with tunable size using a valve-based microfluidic device.* Langmuir, 2014. **30**(42): p. 12610-8.
64. Kamp, J., J. Villwock, and M. Kraume, *Drop coalescence in technical liquid/liquid applications: a review on experimental techniques and modeling approaches.* Reviews in Chemical Engineering, 2017. **33**(1): p. 1-47.
65. Dudek, M., et al., *Microfluidic method for determining drop-drop coalescence and contact times in flow.* Colloids and Surfaces A: Physicochemical and Engineering Aspects, 2020. **586**: p. 124265.

66. Hettiarachchi, K., et al., *On-chip generation of microbubbles as a practical technology for manufacturing contrast agents for ultrasonic imaging.* Lab on a Chip, 2007. **7**(4): p. 463.
67. Niu, X., et al., *Pillar-induced droplet merging in microfluidic circuits.* Lab on a Chip, 2008. **8**(11): p. 1837-1841.
68. Santander-Ortega, M.J., et al., *Colloidal stability of pluronic F68-coated PLGA nanoparticles: a variety of stabilisation mechanisms.* J Colloid Interface Sci, 2006. **302**(2): p. 522-9.
69. Costanzo, S., et al., *Rheology and morphology of Pluronic F68 in water.* Physics of Fluids, 2021. **33**(4).
70. Singla, P., et al., *Advances in the therapeutic delivery and applications of functionalized Pluronics: A critical review.* Advances in Colloid and Interface Science, 2022. **299**: p. 102563.
71. Lee, M.H., G.H. Shin, and H.J. Park, *Solid lipid nanoparticles loaded thermoresponsive pluronic-xanthan gum hydrogel as a transdermal delivery system.* Journal of Applied Polymer Science, 2018. **135**(11).
72. Akash, M.S.H. and K. Rehman, *Recent progress in biomedical applications of Pluronic (PF127): Pharmaceutical perspectives.* Journal of Controlled Release, 2015. **209**: p. 120-138.
73. Escobar-Chávez, J., et al., *Applications of thermo-reversible pluronic F-127 gels in pharmaceutical formulations.* Journal of Pharmacy & Pharmaceutical Sciences, 2006. **9**(3): p. 339-58.
74. Sahu, A., et al., *Encapsulation of curcumin in Pluronic block copolymer micelles for drug delivery applications.* Journal of Biomaterials Applications, 2011. **25**(6): p. 619-639.
75. Jarak, I., et al., *Pluronic-based nanovehicles: Recent advances in anticancer therapeutic applications.* European Journal of Medicinal Chemistry, 2020. **206**: p. 112526.
76. Gioffredi, E., et al., *Pluronic F127 hydrogel characterization and biofabrication in cellularized constructs for tissue engineering applications.* Procedia Cirp, 2016. **49**: p. 125-132.
77. Almeida, H., et al., *Pluronic® F-127 and Pluronic Lecithin Organogel (PLO): Main features and their applications in topical and transdermal administration of drugs.* Journal of Pharmacy & Pharmaceutical Sciences, 2012. **15**(4): p. 592-605.
78. Hernandez, C., et al., *Role of Surface Tension in Gas Nanobubble Stability Under Ultrasound.* ACS Appl Mater Interfaces, 2018. **10**(12): p. 9949-9956.
79. Firestone, M.A., A.C. Wolf, and S. Seifert, *Small-angle X-ray scattering study of the interaction of poly (ethylene oxide)-b-poly (propylene oxide)-b-poly (ethylene oxide) triblock copolymers with lipid bilayers.* Biomacromolecules, 2003. **4**(6): p. 1539-1549.
80. Chen, Z., et al., *Engineering the Echogenic Properties of Microfluidic Microbubbles Using Mixtures of Recombinant Protein and Amphiphilic Copolymers.* Langmuir, 2019. **35**(31): p. 10079-10086.
81. Angilè, F.E., et al., *Recombinant protein-stabilized monodisperse microbubbles with tunable size using a valve-based microfluidic device.* Langmuir, 2014. **30**(42): p. 12610-12618.
82. Frost, H.M., *Electromagnetic–ultrasound transducers: Principles, practice, and applications*, in *Physical acoustics*. 1979, Elsevier. p. 179-275.
83. Correas, J.-M., et al., *Ultrasound contrast agents: properties, principles of action, tolerance, and artifacts.* European Radiology, 2001. **11**: p. 1316-1328.
84. Hilgenfeldt, S., D. Lohse, and M. Zomack, *Response of bubbles to diagnostic ultrasound: a unifying theoretical approach.* The European Physical Journal B-Condensed Matter and Complex Systems, 1998. **4**(2): p. 247-255.
85. Emmer, M., et al., *The onset of microbubble vibration.* Ultrasound in Medicine & Biology, 2007. **33**(6): p. 941-949.
86. Helfield, B., *A Review of Phospholipid Encapsulated Ultrasound Contrast Agent Microbubble Physics.* Ultrasound Med Biol, 2019. **45**(2): p. 282-300.

87. Segers, T., et al., *High-precision acoustic measurements of the nonlinear dilatational elasticity of phospholipid coated monodisperse microbubbles.* Soft Matter, 2018. **14**(47): p. 9550-9561.
88. Abou-Saleh, R.H., et al., *Horizon: Microfluidic platform for the production of therapeutic microbubbles and nanobubbles.* Rev Sci Instrum, 2021. **92**(7): p. 074105.
89. Tremblay-Darveau, C., R. Williams, and P.N. Burns, *Measuring absolute blood pressure using microbubbles.* Ultrasound in Medicine & Biology, 2014. **40**(4): p. 775-787.
90. Owen, J., et al., *The Role of PEG-40-stearate in the Production, Morphology, and Stability of Microbubbles.* Langmuir, 2019. **35**(31): p. 10014-10024.
91. Shih, R. and A.P. Lee, *Post-Formation Shrinkage and Stabilization of Microfluidic Bubbles in Lipid Solution.* Langmuir, 2016. **32**(8): p. 1939-1946.
92. Van Elburg, B., et al., *Feedback-controlled microbubble generator producing one million monodisperse bubbles per second.* Review of Scientific Instruments, 2021. **92**(3): p. 035110.
93. Bąk, A., et al., *Surface properties ofperfluorodecalin–containing liquid/liquid systems: The influence of Pluronic F-68 dissolved in the aqueous phase.* Journal of Fluorine Chemistry, 2018. **215**: p. 36-43.
94. Israelachvili, J.N., *Intermolecular and surface forces*. 2011: Academic Press.